AD NUMBER

AD803189

LIMITATION CHANGES

TO:

Approved for public release; distribution is unlimited.

FROM:

**Distribution authorized to U.S. Gov't. agencies and their contractors;
Administrative/Operational Use; OCT 1966. Other requests shall be referred to Rome Air Developmet Center, RADC/EMLI, Griffiss AFB, NY 13440.**

AUTHORITY

RADC ltr 17 Sep 1971

AD803189

STUDY AND INVESTIGATION OF AN IMPROVED PROTON MASER ANTENNA

Clarence Thornburg
Jonathan Webster
Gordon Guttrich

National Company, Inc.

AFLC, GAFB, N.Y., 27 Nov 66-104

TABLE OF CONTENTS

TABLE OF CONTENTS (Continued)

TABLE OF ILLUSTRATIONS

TABLE OF ILLUSTRATIONS (Continued)

EVALUATION

This effort covers applied research in nuclear magnetic resonance for the improvement of detection sensitivity and for the provision of band tuning for an electromagnetic energy sensor. The small size of this sensor, compared with conventional antennas, makes it usable for the detection of extremely low and very low frequencies in hardened communication complexes where the antenna is buried underground and the transmitted energy propagates through the earth's crust. This effort increased the knowledge in the field of nuclear magnetic resonance applications for practical devices, making the realization of such devices more feasible. The information obtained as a result of this effort will be utilized in the formulation of future work concerned with the utilization of the nuclear magnetic resonance phenomena for survivable communications purposes.

Walter J. Bushunow

WALTER J. BUSHUNOW
Project Engineer

SECTION 1

I N T R O D U C T I O N

1.1 BASIC PROBLEM

We are concerned in this program with the reception of very low frequency electromagnetic waves. The loop antenna has been the traditional apparatus employed in the reception of such signals; however, certain difficulties become apparent as the wavelength of the signals becomes very long.

The rapid deterioration of conventional loop performance as the carrier frequency is reduced results from the unfavorable ratio of the antenna size to the signal wavelength. If ideal reception were to be achieved, the loop should extract all the energy passing within a radius of $\approx \lambda/5$. In practice, the loop may have an effective aperture not much larger than its own physical dimensions. When this picture is couched in electrical terms one says that the radiation resistance of the antenna is negligible compared to its internal ohmic losses. Hence, it is not efficiently coupled to the external radiation field. In particular, the field strength must exceed a minimum value so that the fraction of signal power intercepted is greater than the internally generated kTB noise power.

Very simply, since the induced Emf is proportional to the rate of change of the flux through the loop, the detected Emf will be inversely proportional to the wavelength. Therefore, for a fixed field strength, there is a minimum detectable frequency below which the signal will be masked by internal thermal noise.

One solution to these problems was the Promant Technique developed by National Company.

1.2 HISTORY OF PROMART

The Promant concept was a result of National Company's previous experience with nuclear magnetic resonance (see Reports RADC-TR-61-132, AD 266 071 and RADC-TDR-63-25, AD 297 920). Basically, the unit consists of a proton maser which is frequency modulated by the direct interaction of the electromagnetic field with dynamically polarized protons. The resulting sidebands are processed and detected to reconstitute the original signals.

By appropriate frequency multiplication and FM detection, even very low indices of modulation of the maser can be detected. The sideband power (for a given signal strength) is directly proportional to the maser power. Hence the useful signal power in the sidebands can greatly exceed that which the loop might have extracted from the passing wavefront. Since both sensors are competing against the same fundamental kTB Johnson noise, the potentialities of the Promant scheme can be appreciated. Furthermore, the nature of the FM sideband power is such that as the signal carrier frequency is reduced, the Promant detection capability is <u>increased</u>. Hence this technique takes over just where the conventional loops are falling off.

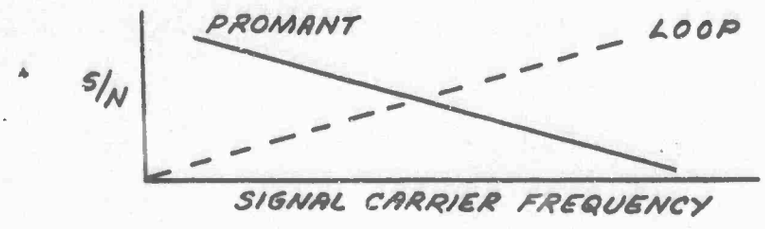

A breadboard model Promant was constructed by National Company under a previous contract (see report RADC-TR-64-567, AD 619 043). The response was studied and compared to the theoretically expected results and it was found possible to observe signals of about 10^{-6} gauss at 100 Hz with a bandwidth of 2.5 Hz and a signal-to-noise ration of unity. The sensitivity was also observed to decrease with increasing carrier frequency as expected.

For VLF detection purposes it would be desirable to receive signal amplitudes in the 10^{-12} gauss range. It would also be desirable to have some means of extending the good low frequency sensitivity to higher frequencies.

This report describes the results of a study and investigation of techniques which showed promise of being the means for achieving these goals. Since most of the necessary theory has been developed in the preceding reports mentioned above, only the necessary results and not the theory will be repeated here. In addition, circuit diagrams and drawings of parts contained in the earlier reports will be omitted.

1.3 PROPOSED IMPROVEMENTS

1.3.1 Increased Sensitivity

In order to respond to the request for proposals to improve the performance of the original Promant, National Company made a thorough search for all methods which could lead to increased sensitivity. This search uncovered two major possibilities and a host of minor ones.

One major possibility was to obtain increased sensitivity by increasing the operating frequency of the maser. The maser power is proportional to the square of the frequency of operation, and since the minimum detectable field is inversely proportional to the square root of

the maser power, we find that the minimum detectable field is inversely proportional to the frequency of operation. In other words, if the maser frequency is doubled, the sensitivity will be doubled. It was predicted that a practical improvement of 30 db could be obtained by this method.

Increasing the maser frequency by a large factor would entail a complete rebuilding of the whole Promant device, an operation which would be quite expensive and time consuming. The increase of maser power with operating frequency was, furthermore, a well established fact, both theoretically and experimentally. For these two reasons, it was not proposed to investigate this means of increasing the Promant sensitivity.

The second major possibility for increasing the sensitivity involved pulsed oscillator operation. It was well understood that the population inversion of the atoms entering the NMR coil represented the influx of a certain amount of potential energy per unit time and that the maximum average power of the oscillator could not exceed that rate of influx of energy. On the other hand, it was felt that this energy could be extracted at any rate during short separated intervals so long as the above average was not exceeded. These relatively high power pulses would then be much easier to detect against the kTB background. It was expected that a practical improvement of up to 38 db could be obtained in this manner.

This pulsed operation, which promised so much improvement and yet was not well understood, even theoretically, was clearly the area that should receive primary emphasis in any investigation of means for improving the sensitivity of Promant. It was therefore proposed that the investigation would be directed toward a study of the pulsing technique.

The more important of the minor possibilities for sensitivity

improvement included (1) modifications of the flux concentrators, (2) reduction of amplifier noise figure and, (3) larger Overhauser enhancement. Although a practical limit of 34 db improvement from these sources was estimated, only an incidental effort to incorporate some of these features was proposed, since it was felt that such optimizations could be made after the basic principles were proved.

If all of the above methods were applied and behaved as theoretically predicted, it was possible that the improved Promant could have a sensitivity of 10^{-11} gauss (100 Hz carrier, 2.5 Hz bandwidth); however, if the pulsing technique failed, the sensitivity would be limited to 10^{-9} gauss, making the device of questionable usefulness as a VLF antenna.

1.3.2 Band Tuning of Antenna

In order to provide a means for extending the good low frequency sensitivity of Promant to higher frequencies, National Company proposed a heterodyning scheme using a mu-switched version of Promant. It was planned to develop this method of tuning to produce a system which could be included in a practical device. A model using this practical method was to be built and tested experimentally.

SECTION 2

PROBLEMS INVESTIGATED

2.1 TECHNIQUES FOR IMPROVING DETECTION SENSITIVITY

2.1.1 Fundamental Concepts

If we define the minimum detectable signal H_m by the condition that the signal-to-noise ratio be unity, then since

$$\frac{1}{2}\left(\frac{\gamma}{2\pi}\frac{\mu_{eff} H_m}{f_s}\right)^2 P_o = kTBF \qquad (2\text{-}1)$$

where P_o is the maser power, F is the amplifier noise figure, and f_s is the "carrier" frequency, and it is assumed that the sidebands are not within 1/2 absorption linewidth of the center frequency, we have the relation:

$$H_m = \frac{\pi(\Delta\nu)_{abs}}{\gamma\,\mu_{eff}}\sqrt{\frac{kTBF}{P_o}} \qquad (2\text{-}2)$$

where f_s has been replaced by $(\Delta\nu)_{abs}/2$ which (see previous reports) gives the minimum value for H_m. Recall also that the maximum value for P_o is:

$$P_o = \left(\frac{1}{2}\right)\frac{N_o A(\hbar\omega_o)^2}{2\,kT}\cdot\frac{\eta V}{2T_1^*} \qquad (2\text{-}3)$$

where N_o is the number of spins per unit volume, ηV is the effective volume of the sample, A is the Overhauser enhancement, T_1^* is the spin lattice relaxation time corrected for flow rate, and ω_o is the operating frequency of the maser. It is assumed here that $Q_T = 2\,Q_{min}$ to give the maximum power without causing maser pulsations. Using $\omega_o = \gamma H_o$ and combining the above, we can obtain a fundamental expression for H_m:

$$H_m = \frac{2\,kT}{\hbar\gamma^2 T_2\,\mu_{eff}\,H_o}\sqrt{\frac{2\,T_1^*\,BF}{N_o\,A\,\eta V}}\left(1+\frac{\gamma\varepsilon H_o T_2}{2}\right) \qquad (2\text{-}4)$$

where the substitution:

$$(\Delta\nu)_{abs} = \frac{\gamma\varepsilon H_o}{2\pi} + \frac{1}{\pi T_2}$$

was used, and where ε is the relative inhomogeneity of the magnetic field over the sample volume.

2.1.2 Improved CW Operation

There are several physical parameters which determine the performance of the proton maser antenna.

(a) Field Strength: From Equation (2-4) we see that H_m is inversely proportional to the DC magnetic field H_o. The field used in the original Promant was only 234 gauss ($\frac{\omega_o}{2\pi}$ = 1 MHz) and since fields of 7,000 gauss ($\frac{\omega_o}{2\pi}$ = 30 MHz) appear practical for such a device, an improvement of 30 db in sensitivity may be obtained by increasing the DC field strength. It should be noted that the full advantages of increasing the DC field strength will not be realized unless the absolute inhomogeneity (εH_o) is controlled, so that the quantity:

$$(1 + \frac{\gamma\varepsilon H_o T_2}{2})$$

occurring in Equation (2-4) is not increased significantly. In general, this requirement will mean that the relative inhomogeneity ε of the stronger magnet must be considerably less than that of the original magnet. As explained previously, major modifications of the magnet were not included in the scope of this program.

(b) Sample Volume: An increase in the effective volume of the sample can be accomplished either by improving the filling factor η or by actually enlarging the sample. Either method will yield an increase in the sensitivity by a factor equal to the square root of the ratio of the new effective volume to the original, i.e., if the effective volume is increased to four times

its original value, the sensitivity will be doubled. In most cases an increase in effective volume will be accompanied by an increase in the relative inhomogeneity ε, and care must be exercised to prevent this adverse effect from cancelling the improvements that would be attained otherwise.

In the course of this program, a new coil box was installed which gave an increase of 50% in the effective volume - an alteration which theoretically increased the sensitivity by 22%. The drawing of this new coil box is shown in Figure 2-1 and should be compared with Figure 3 of the preceding report (RADC-TR-64-567).* Note the larger sample volume and the increased length of the UHF helix. A photograph of the completed coil box is shown in Figure 2-2, whereas a photograph of the original coil box was shown in Figure P-1 of Appendix B in the report mentioned above.

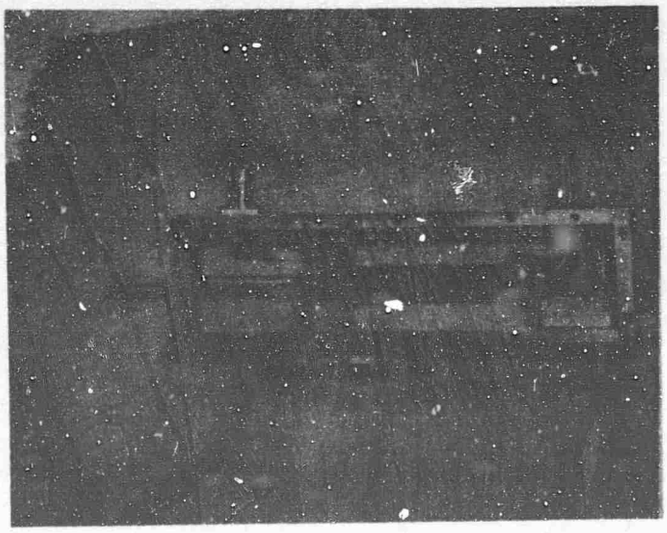

Figure 2-2 - The New Coil Box

*AD 619 043

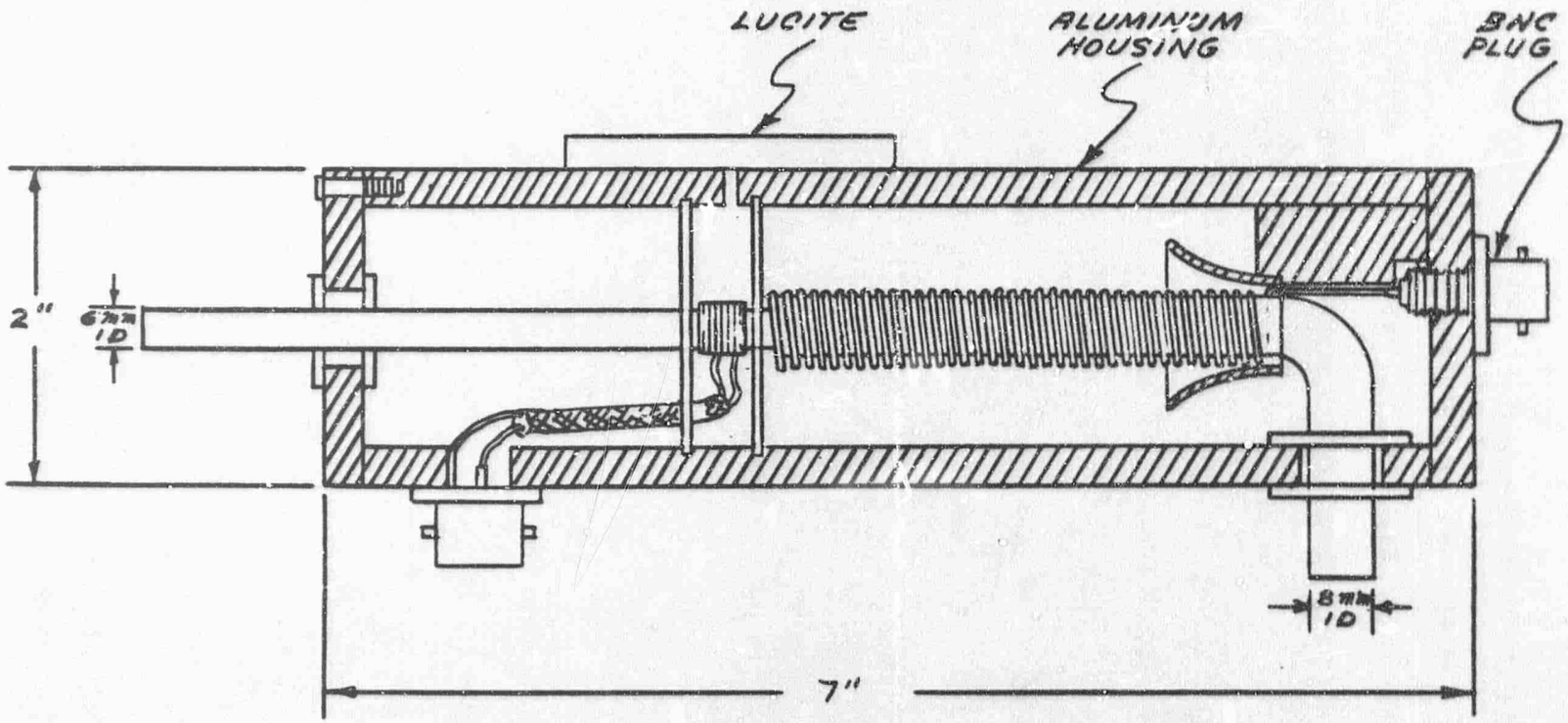

Figure 2-1 - Drawing of the New Coil Box

(c) Temperature: Although it appears that the sensitivity is very simply dependent on the absolute temperature, such is not the case. Almost every parameter appearing in Equation (2-4) has some temperature dependence. Some of these effects can be neglected; however, others may be quite important. For instance, if the viscosity of the liquid changes as a result of a temperature change, we would expect changes in both T_1 and T_2; furthermore, if the flow rate changes as a result of the viscosity change, T_1^* will be further altered. The general effect of a viscosity increase is to broaden the absorption linewidth, thereby decreasing the sensitivity.

It was found that the parameter most sensitive to temperature was the Overhauser enhancement, A. This dependence was to be expected in the present case as free radicals were used for the ESR pumping and the number of unpaired electrons depends strongly on temperature. In one experiment, an increase in temperature from 25° C to 50° C doubled the Overhauser enhancement. Since the Overhauser enhancement is limited in value, the temperature variation to be expected would depend not only on the type of ESR substance used, but also on the original enhancement.

Finally, there is the direct temperature dependence which, if not masked by the side effects described above, gives increased sensitivity for a decrease in temperature.

Because of the difficulty of using cryogenic measures in any practical device, the effects of a variation of temperature were not examined in the proton maser antenna.

(d) Overhauser Effect: An Overhauser enhancement of A = 55 was obtained in the original Promant. If this enhancement could be increased to its ultimate limit (A = 330) without altering the relaxation times (T_1 and T_2),

the sensitivity would be improved by a factor of 2.4. An improvement of this size could not be realized in practice for several reasons: the relaxation times may indeed be affected, and the practical limit to the Overhauser effect in a flowing system appears to be about A = 250.

The Overhauser enhancement in a free radical bearing sample is given by $A = -(1/2)(F/m)\frac{S}{S+1}(\gamma_e/\gamma_p)$, where F is the efficiency, m the weighted multiplicity of the ESR line, and S is the electron resonance saturation factor. γ_e and γ_p are, respectively, the gyromagnetic ratios of the electrons and protons.

The efficiency F varies between 0 and 1 and represents the relative contribution of the excited free radicals to the total relaxation processes of the protons. It is given by $F = 1 - (T_1/T_{1_0})$, where T_1 and T_{1_0} are the proton longitudinal relaxation times with and without free radicals. Thus, F is determined by measuring T_1 and T_{1_0}. This has been done by photographing the buildip of the NMR line after the removal of a saturating H_1 field. The results are tabulated below:

	T_1	F	A_{max}	Figure
Ethyl alcohol (denatured)	1.4 ± .1 sec	-	-	2-3
Ethyl alcohol with NaOH	1.2 ± .1	-	-	2-4
TCS - 5 minutes	.75 ± .03	.25	-76 ± 40%	2-5
- 30 minutes	.5 ± .1	.5	-165 ± 20%	2-6
- 2 hours	.3 ± .07	.7	-230 ± 20%	2-7
Dead TCS (heat treated)	1.0 ± .1	0	0	2-8

A_{max} is the maximum theoretical enhancement assuming complete saturation. Typical enhancements reported for the operational Proxant were A = -50 or only 22% of this maximum value.

Figure 2-3 - Ethyl Alcohol (denatured) - (sweep rate: 1 sec/cm)

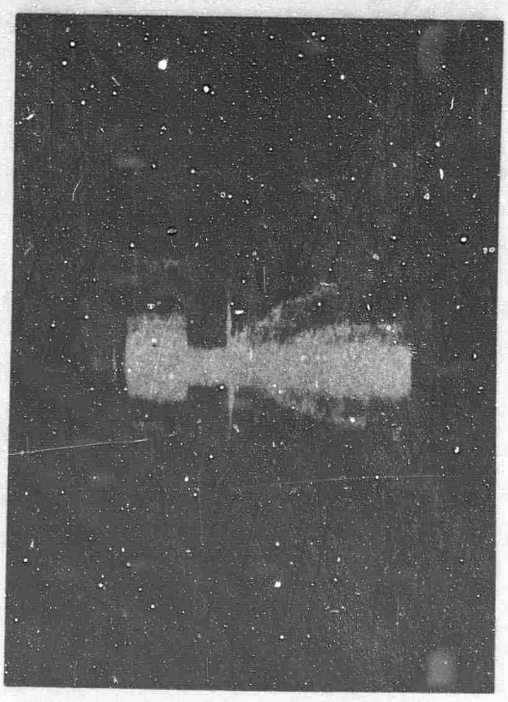

Figure 2-4 - Ethyl Alcohol with NaOH (sweep rate: 0.5 sec/cm)

Figure 2-5 - TCS-5 minutes after preparation (sweep rate: 0.5 sec/cm)

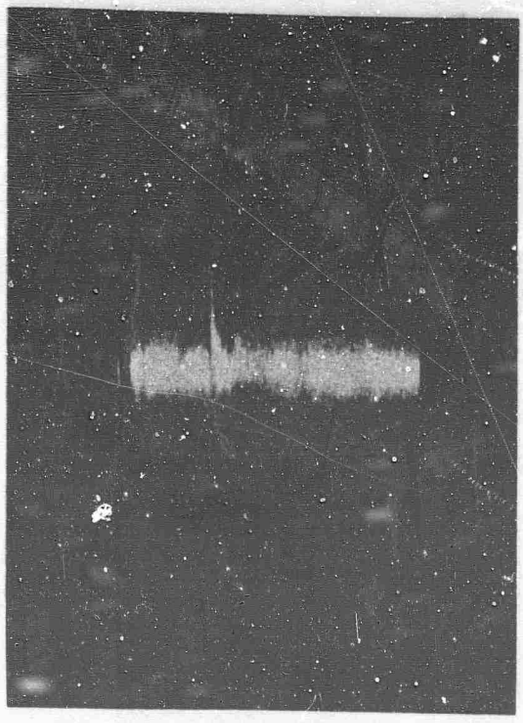

Figure 2-6 - TCS-30 minutes after preparation (sweep rate: 0.2 sec/cm)

Figure 2-7 - TCS-2 hours after preparation (sweep rate: 0.5 sec/cm)

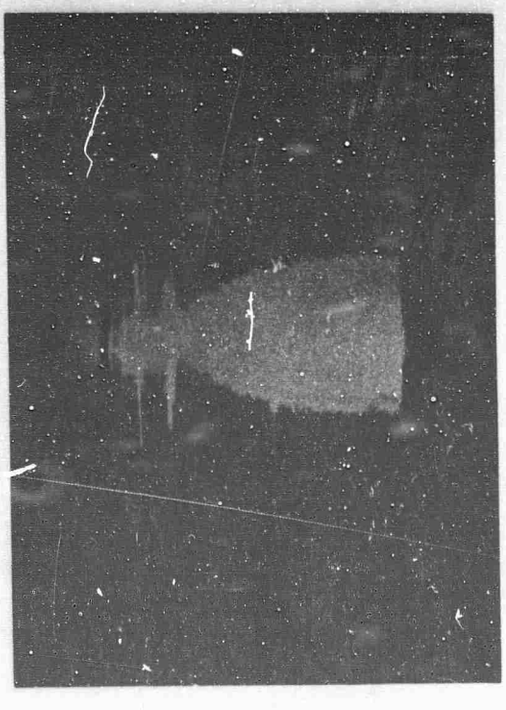

Figure 2-8 Dead TCS (sweep rate: 0.5 sec/cm)

We ascribe this deficiency partly to the inadequate time spent by the sample in the UHF helix. The measured relaxation times and flow velocities for maximum power in the operational Promant indicate Overhauser enhancements of -50 to -100; typical enhancements were about -50 to -55.

Two attempts were made at 3.3 K gauss to realize the full Overhauser magnetization indicated by F. In one experiment, a small quantity of sample was exposed for a time $t >> T_{1e}$ to the saturating microwave field. Then this fully magnetized sample was suddenly injected into the NMR coil and the resulting pulse photographed. Enhancements in excess of -250 were indicated in this way, but the measurements were not consistent and are viewed with suspicion (see Figure 2-9). The second experiment employed a stationary sample and a microwave permeable NMR coil. A thermocouple immersed in the sample showed that the strongest heating effect occurred within the NMR coil. Enhancements of about -80 were observed with no flow. Records of the enhancement and sample temperature versus time measured from the application of microwave power show an initial short rise time and a much longer rise time and, finally, a magnetization decay - see Figure 2-10 (magnetization decay not shown).

In addition to relaxation time studies, modifications were made in the unit itself to provide increased Overhauser enhancement. The most important modification was the new coil box described above (Figure 2-1) which provided for improved electron resonance saturation by means of a longer UHF helix. At first the full potential of this new helix could not be realized because of a lack of sufficient driving power at the UHF frequencies, but after an oscillator capable of the required 4 watts was obtained, Overhauser enhancements in the range of 75 to 90 were observed.

Figure 2-9 - Overhauser enhancement of 250 (pulse attenuated by 2.5)

Figure 2-10 - Overhauser enhancement for no flow (lower trace is temperature at 5°C/cm starting at 27°C-sweep rate is 2 sec/cm right-to-left)

This improved enhancement corresponds to a 25% theoretical increase in sensitivity.

(e) Double Frequency Narrowing: The technique of line narrowing by double frequency irradiation appeared to be an attractive means for obtaining increased maser power and, thereby, improving the sensitivity. This phenomena was first observed by Sarles and Cotts[1] and was explained theoretically for the case of solids by Bloch.[2] These investigations have recently been extended to the case of liquids by Jha[3] who derived the field conditions for narrowing.

The double frequency technique is quite similar to the motional-narrowing technique in which the sample is mechanically rotated to average the field inhomogeneities, thereby giving a narrower line. In the double frequency technique, one field is the ordinary r.f. field applied to the sample, while the other is a very strong rotating field, the effect of which can be represented by an effective rotation of the spins. The dipolar broadening of the resonance line may be quenched by this method, resulting in a narrower line. The narrowing of the line, in turn, allows the use of a sample with a smaller T_1, yielding a larger oscillator power (see Equation 2-3; it is anticipated that a spin oscillator rather than a maser would be required here because of the presence of the second r.f. field; however, the power equation has essentially the same form for both cases).

Unfortunately, the rotating r.f. field required to produce substantial narrowing is far too large to be practical - of the order of kilogauss

---

[1] Sarles and Cotts, Phys. Rev. 111, 853 (1958)
[2] Bloch, Phys. Rev. 111, 841 (1958)
[3] Jha, J. Phys. Soc. Japan, 21, 42 (1966)

(see the article by Jha). Moreover, the effects of such a large r.f. field on the Overhauser enhancement are not known and cannot be easily estimated. Because of these difficulties, this technique is considered only of academic interest at the present time.

2.1.3 Pulsed Operation

(a) Expected Performance: Prior to the rigorous analysis presented in paragraph (b) below, it was thought that the energy stored in a nuclear spin system could be extracted at an arbitrarily large rate. It was realized that the inverted population represented a certain amount of potential energy per unit volume and because of the flow, this energy arrived at the NMR coil at a certain rate. Therefore, the average power that could be extracted from the spins was definitely limited. On the other hand, it was believed that the energy could be extracted in short, separated, high-power pulses. Even the simple quantum mechanical picture did not contradict this belief. The error lay in the concept of considering the quantum states of each of the spins separately; whereas, a rigorous treatment required the realization that all of the spins formed a "Super Quantum State". A more rigorous theory of pulsed operation which accounts for this Super Quantum State is presented herewith.

(b) Theory of Pulsed Operation: It has been shown[4] from first principles that for all relaxation mechanisms normally encountered in a liquid such as dipolar couplings between like spins or fluctuating quadrupole coupling with extreme narrowing, that the macroscopic nuclear magnetization of these liquid systems should obey the Bloch Equation in the absence of an

---

[4] Abragam, "Nuclear Magnetization", Oxford 1961, Chapter 3 and page 511

applied r.f. field. It can further be shown[5] that for liquids, if the Bloch equations are valid in the absence of an r.f. field, they will still be valid with the same relaxation times in the presence of such a field of amplitude H_1, provided $|\gamma H_1| \tau_c \ll 1$ (non-viscous liquids). If we take $\tau_c \sim 10^{-11}$ sec., for a liquid sample[6], then an oscillating field $H_{osc} = 2H_1 = \frac{2}{2\pi \times 4 \times 10^3 \times 10^{-11}} \sim 8 \times 10^6$ gauss is required to affect the relaxation times. Since this is clearly an impractical field strength to attain, we may assume that the Bloch equations will always apply to ordinary liquid samples. For the present problem, the use of liquid materials is indicated because of the unacceptably broad linewidths encountered with solids.

The Bloch equations may be written:[7]

$$\frac{d\vec{M}}{dt} = \gamma \vec{M} \times \vec{H} - \frac{M_x \vec{i}' + M_y \vec{j}'}{T_2} - \frac{M_z - M_0}{T_1} \vec{k}' \qquad (2\text{-}5)$$

where $\vec{i}'$, $\vec{j}'$, and $\vec{k}'$ are the unit vectors in the lab frame and M_x, M_y and M_z are the respective components of the magnetization.

Assume that the applied field is the sum of a DC field $H_z = H_0 = -\frac{\omega_0}{\gamma}$ and an r.f. field $\vec{H}_1$ with $|\vec{H}_1| = -\frac{\omega_1}{\gamma}$ rotating at a frequency ω, $\omega \sim \omega_0$. (This is, in our case, one of the rotating components of the applied field, $H_x = 2 H_1 \cos \omega t$, linearly polarized along the x axis in the laboratory frame; the effect of the counter-rotating component is neglected). In the frame rotating about H_0 at the frequency ω_1, there is an effective static field:

---

[5] ibid, p. 517

[6] Bloembergen, "Nuclear Magnetic Resonance", New York 1961., p. 90

[7] ibid, p. 45

$$\vec{H}_{eff} = \left(H_0 + \frac{\omega}{\gamma}\right)\vec{k} + H_1\vec{i} = \frac{\Delta\omega\,\vec{k} - \omega_1\vec{i}}{\gamma} \qquad (2\text{-}6)$$

where i, j, k = k' (a frame rotating about the z axis) are the unit vectors in the rotating frame and

$$\omega_0 = -\gamma H_0 \;,\; \omega_1 = -\gamma H_1 \;,\; \Delta\omega = \omega - \omega_0 \qquad (2\text{-}7)$$

Then in the rotating frame the equation of motion is:

$$\frac{d\vec{M}'}{dt} = \gamma(\vec{M} \times \vec{H}_{eff}) - \frac{M_x'\vec{i} + M_y'\vec{j}}{T_2} - \frac{M_z - M_0}{T_1}\vec{k} \qquad (2\text{-}8)$$

where M_x' and M_y' are the transverse components of M in that frame. Writing this equation in component form, we have:

$$\begin{aligned} \frac{dM_x'}{dt} &= -\frac{M_x'}{T_2} + \Delta\omega M_y' \\ \frac{dM_y'}{dt} &= -\Delta\omega M_x' - \frac{M_y'}{T_2} - \omega_1 M_z \\ \frac{dM_z}{dt} &= \omega_1 M_y' - \frac{M_z - M_0}{T_1} \end{aligned} \qquad (2\text{-}9)$$

To study the behavior of the components of the magnetization rotating at the applied frequency ω, we must solve these coupled differential equations. Since we are interested in the transient behavior of the system, let us solve these equations using the method of Laplace transforms, which is the most convenient method for this type of problem.

For convenience, define:

$$V = M_z' - M_0 \qquad (2\text{-}10)$$

Now,

$$\begin{aligned} \dot{M}_x' &= -\frac{M_x'}{T_2} + \Delta\omega M_y' \\ \dot{M}_y' &= -\Delta\omega M_x' - \frac{M_y'}{T_2} - \omega_1 V + \omega_1 M_0 \\ \dot{V} &= \omega_1 M_y' - \frac{V}{T_1} \end{aligned} \qquad (2\text{-}11)$$

Define:

$$L\,(M_x'(t)) = m_x(s)$$
$$L\,(M_y'(t)) = m_y(s) \qquad (2\text{-}12)$$
$$L\,(V(t)) = v(s)$$

where $L\,(F(t)) = \int_0^\infty e^{-st} F(t)\,dt$ = the Laplace transform of F(t).

Let us consider the solution of the Bloch equations in response to a unit step of r.f. field. The turn-off of the field will produce only exponentially decaying terms, and will add no information related to possible enhancement through pulsing.

$$H_1(t) = [H_1 \sin \omega t]\,u(t), \qquad u(t) = \begin{cases} 0, & t<0 \\ 1, & t>0 \end{cases} \qquad (2\text{-}13)$$

This can equivalently be written:

$$H_1(t) = H_1 \sin[\omega(t)\,t], \quad \text{where } \omega(t) = \omega\,u(t) \qquad (2\text{-}14)$$

Then in the above equations, $\Delta\omega(t) = \omega(t) - \omega_o$, and

$$L(\Delta\omega(t)\,M_i) = \int_0^\infty e^{-st}[\omega\,u(t) - \omega_o]\,M_i\,dt$$
$$= \int_0^\infty e^{-st}(\omega - \omega_o)\,M_i\,dt \qquad (2\text{-}15)$$
$$= \Delta\omega\; m_i(s)$$

Now:

$$L\left[\frac{dF(t)}{dt}\right] = s\,f(s) - F(o) \qquad (2\text{-}16)$$

Before t = 0, $M_x' = M_y' = 0$, $M_z' = M_o$ and $\therefore$ V = 0.

Therefore, the Laplace transforms of the equations are:

$$s\,m_x(s) = -\frac{m_x(s)}{T_2} + \Delta\omega\, m_y(s)$$

$$s\,m_y(s) = -\Delta\omega\, m_x(s) - \frac{m_y(s)}{T_2} - \omega_1 v(s) - \frac{\omega}{s} M_0 \qquad (2\text{-}17)$$

$$s\,v(s) = \omega_1 m_y - \frac{v(s)}{T_1}$$

or,

$$\begin{pmatrix} -\frac{1}{T_2} - s & \Delta\omega & 0 \\ -\Delta\omega & -\frac{1}{T_2} - s & -\omega_1 \\ 0 & \omega_1 & -\frac{1}{T_1} - s \end{pmatrix} \begin{pmatrix} m_x \\ m_y \\ v \end{pmatrix} = \begin{pmatrix} 0 \\ \frac{\omega_1}{s} M_0 \\ 0 \end{pmatrix} \qquad (2\text{-}18)$$

Solving for m_y,

$$m_y(s) = \frac{\omega_1 \left(s + \frac{1}{T_2}\right)\left(s + \frac{1}{T_1}\right) M_0}{s\,\xi} \qquad (2\text{-}19)$$

$$\xi = -\left(\frac{1}{T_2} + s\right)^2 \left(s + \frac{1}{T_1}\right) - \omega_1^2 \left(s + \frac{1}{T_2}\right) - (\Delta\omega)^2 \left(s + \frac{1}{T_1}\right)$$

Assume $T_1 = T_2 = T$ (valid for a liquid):

$$m_y = \frac{-\left(s + \frac{1}{T}\right) M_0 \omega_1}{s\left[\left(s + \frac{1}{T}\right)^2 + \omega_1^2 + (\Delta\omega)^2\right]} \qquad (2\text{-}20)$$

let $a = \frac{1}{T}$, $\quad b = \left[\omega_1^2 + (\Delta\omega)^2\right]^{\frac{1}{2}}$

$$m_y = -M_0 \omega_1 \frac{s+a}{s\left[(s+a)^2 + b^2\right]}$$

$$m_y = -M_0 \omega_1 \frac{s+a}{s(s+a+ib)(s+a-ib)} \qquad i = \sqrt{-1} \qquad (2\text{-}21)$$

$$m_y = -M_0 \omega_1 \left[\frac{1}{(s+a+ib)(s+a-ib)} + \frac{1}{s(s+a+ib)(s+a-ib)}\right.$$

Taking the inverse transform of this expression, we find:

$$M_y' = -\frac{M_0 \omega_1 T}{1+(\omega_1 T)^2+(\Delta\omega T)^2}\left[1 - e^{-\frac{t}{T}}\left(\cos\omega_\tau t - T\omega_1 \sin\omega_\tau t\right)\right] \qquad (2\text{-}22)$$

where $\omega_\tau = \left[\omega_1^2 + (\Delta\omega)^2\right]^{1/2}$

$\omega_1 = \gamma H_1$

$\Delta\omega = \omega - \omega_o$, where $\omega_o = \gamma H_o$ and ω is the frequency of the applied r.f. field.

Suppose we apply the step of r.f. field at resonance, then:

$$m_y' = -\frac{M_0 \omega_1 T}{1+(\omega_1 T)^2}\left[1 - e^{-\frac{t}{T}}\left(\cos\omega_1 T - \omega_1 T \sin\omega_1 T\right)\right] \qquad (2\text{-}23)$$

This coefficient, $\frac{-M_0 \omega_1 T}{1+(\omega_1 T)^2}$ is the response to a CW r.f. field, and the damped sinusoidal term represents the transient response characteristics. m_y' has its maximum at $t = \frac{\pi}{2\omega_\tau}$, with a value,

$$m_{y\,\max}' = -\frac{M_0 \omega_1 T}{1+(\omega_1 T)^2}\left[1 + \omega_1 T\, e^{-\frac{\pi}{2\omega_1 T}}\right] \qquad (2\text{-}24)$$

$$= m_{y\ \text{steady state}}'\left(1 + \omega_1 T\, e^{-\frac{\pi}{2\omega_1 T}}\right)$$

where $m_{y\ \text{steady state}}' = \frac{-M_0 \omega_1 T}{1+(\omega_1 T)^2}$

We see that M_y' steady state has its maximum at $\omega_1\tau = 1$ with a value $M_{y\,s.s.}' = -\frac{1}{2}M_o$. $M_{y\,max}'$, however, exceeds this value, increasing linearly from zero for small $\omega_1\tau$, and approaching a value of $-M_o$ for large $\omega_1\tau$.

$$\lim_{\omega_1\tau \to \infty} M_{y'_{max}} = -M_o$$

For $\omega_1\tau = 1$, corresponding to the value of the field for the maximum steady state magnetization, the magnitude of this maximum overshoot has reached

$$M_{y\,max}' (\omega_1\tau = 1) \approx 0.6\, M_o .$$

$$M_{y\,max}' (\omega_1\tau = 5) \approx 0.9\, M_o . \qquad (2\text{-}25)$$

From this calculation, it is clear that the maximum increase in signal amplitude that can be achieved by pulses of r.f. field over a CW method is a factor of two in terms of the magnitude of the rotating magnetization at the resonant frequency.

(c) Experimental Verification: Several experiments were performed to verify these results. The experimental arrangement is shown in Figure 2-11.

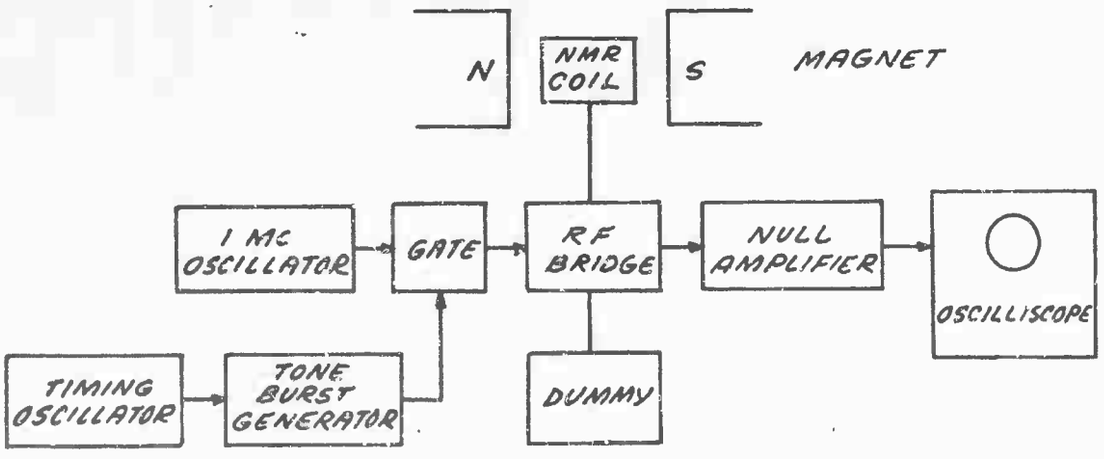

Figure 2-11 - Experimental Arrangement for Pulsing Tests

The various components used here are described in detail in Section 3.2. The traces on the oscilloscope were photographed and are reproduced below

The first set of photographs show the effects of a change in r.f. power level on the ringing signal that is obtained during pulsing. Since the ringing frequency is equal to ω_τ and since $\omega_\tau = \sqrt{(\gamma H_1)^2 + \Delta\omega^2}$, we would expect ω_τ to increase with increased r.f. level, i.e., we would expect the frequency of the ringing to be higher for a higher r.f. level. In Figure 2-12 (b), the r.f. level is larger than that in Figure 2-12 (a); note the difference in frequency (the sweep speed is the same).

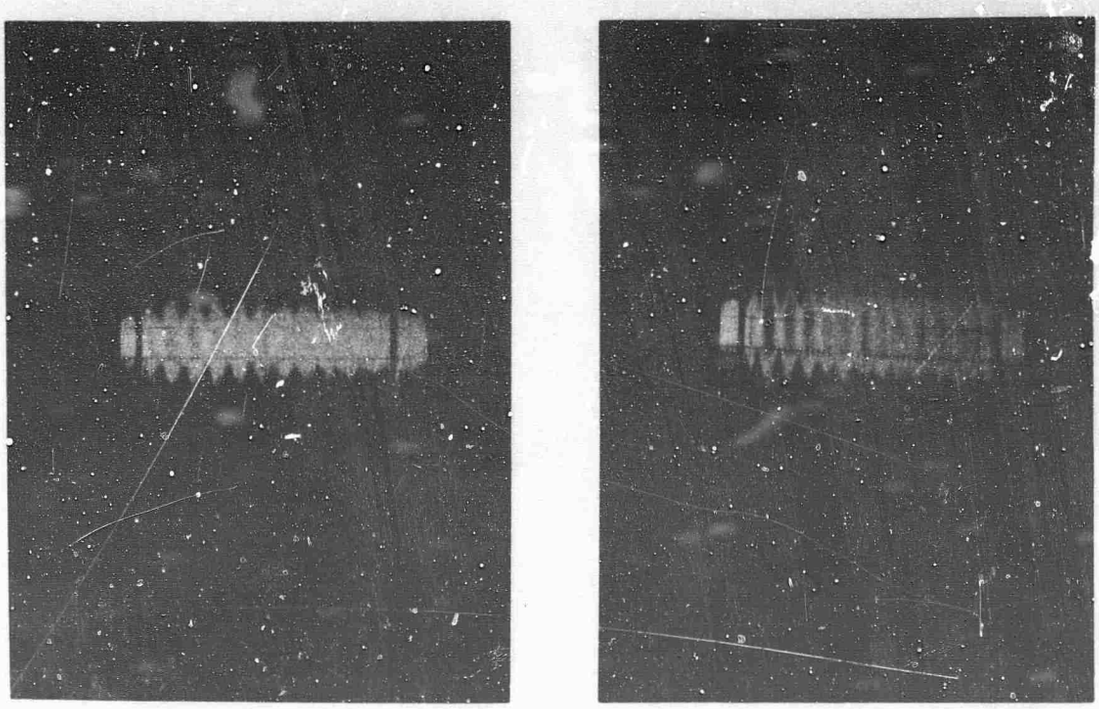

(a) r.f. input to bridge=0.5 volt (b) r.f. input to bridge=1.2 volt

Note: Not precisely on resonance; no H_o field change between pictures.

Figure 2-12 - Effect of r.f. level on Ringing Frequency

The second set of photographs show the behavior of the ringing signal as the H_o field (i.e., $\Delta\omega$) is changed. Here we expect ω_τ to decrease as resonance is approached (i.e., $\Delta\omega \rightarrow 0$). Figure 2-13 (a) shows the response off resonance; whereas Figure 2-13 (b) shows the response on resonance (i.e., $\Delta\omega = 0$); note that the ringing frequency is higher off resonance, as expected.

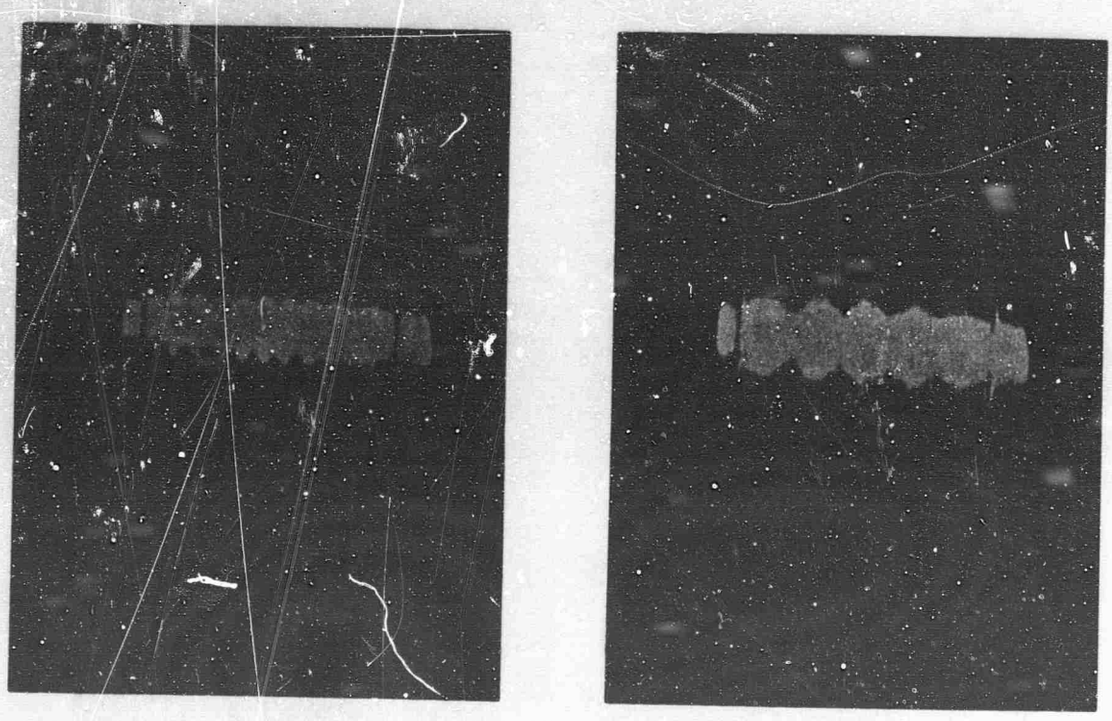

(a) off resonance (b) on resonance

Note: Same r.f. field for both pictures; r.f. input to bridge = 0.4 volts

Figure 2-13 - Effect of Magnetic Field Change on Ringing Frequency

The third set of photographs emphasize the ring-down pattern. After a pulse, the magnetization vector is left tipped over and a decaying signal will be induced in the pickup coil. Since there is no input to the bridge

the ring-down will look the same independent of the bridge adjustment. In Figure 2-14 (a), the bridge is adjusted normally; whereas, in Figure 2-14 (b), the bridge is misadjusted just enough to null out the pulse. Note that the ring-down looks the same in both instances, as expected.

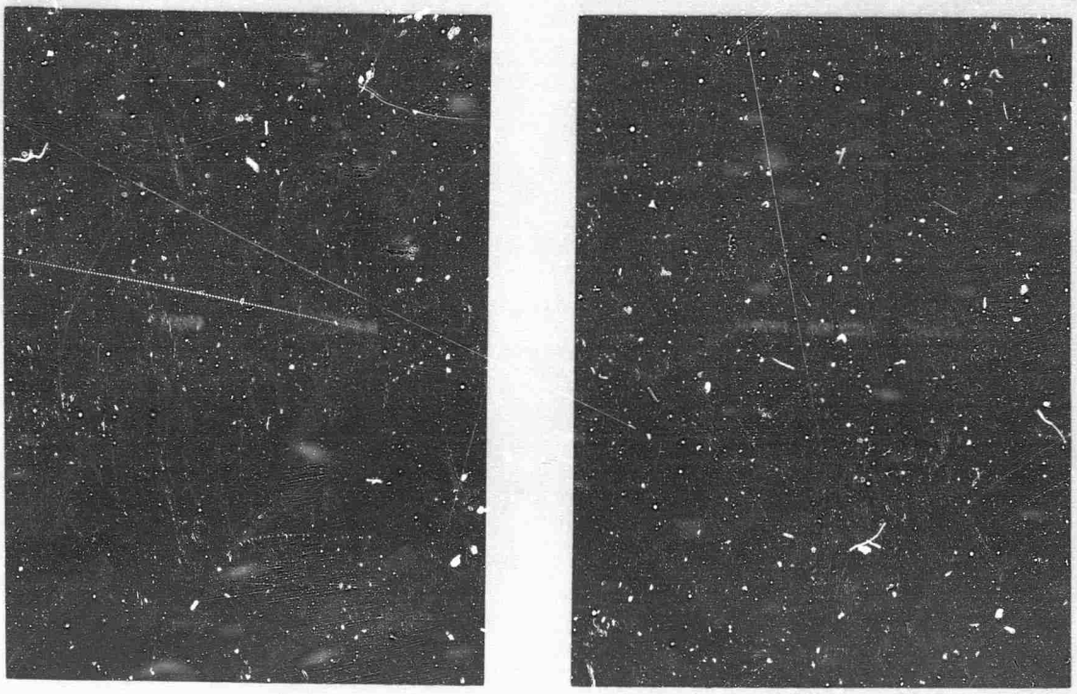

(a) bridge normal (b) bridge adjusted to cancel NMR signal

Note: All other conditions are the same for both pictures

Figure 2-14 - The Independence of the Ring-down on the Bridge Balance

The agreement between the experimental results and the theoretical predictions is very good. The combination of the two leaves no alternative to the conclusion that pulsing is not beneficial, i.e., pulsing produces no increase in the maximum instantaneous power which can be attained.

2.1.4 Electronic Techniques

Some of the techniques available for improving the performance of the proton maser antenna are of a primarily electronic nature and thus depend on the state-of-the-art of the various electronic components.

(a) Effective Permeability: The sensitivity of the antenna is directly proportional to the effective permeability. However, with the present apparatus, increases in the effective permeability gained by moving the flux concentrator rods nearer to the magnet are accompanied by an increase in the inhomogeneity of the DC magnetic field. Although an effective permeability of 10 can be achieved, the field has a useable homogeneity only for $\mu_{eff} < 6$. Techniques used to overcome these difficulties by adding small magnets to the flux concentrators will be discussed in a later section. This later section also contains a description of the dynamic flux concentrators and curves showing the improvements obtained over the original configuration.

(b) Magnetic IF: The use of the techniques described in Section 2.2 below to produce a magnetic IF at a frequency of

$$f_{IF} = \frac{1}{2} (\Delta\nu)_{abs}$$

permits almost maximum sensitivity to be obtained over a wide range of frequencies.

(c) Amplifier Noise Figure: There was approximately a factor of 10 difference between the theoretically predicted performance of the original Promant (assuming an electronics noise figure of unity) and the experimentally measured sensitivity. If all of this difference is assigned to the electronics noise figure, the value obtained is 20 db. Some part of this number arises from the phase fluctuations in the multiplier chain, other internally generated noises and noises picked up from external sources in the electronics

following the initial amplifier, and the remainder arises from the internal noise of the initial amplifier. Therefore it was possible that the original amplifier could have had a noise figure as bad as 15 db, which is approximately 10 db worse than the state-of-the-art for amplifiers without positive feedback. A considerable amount of effort (in the light of the maximum possible improvement in sensitivity - less than a factor of 3) was expended in attempts to improve the noise properties of the amplifier.

These attempts included the design and construction of an amplifier employing low noise field effect transistors. The field effect transistor amplifier was found to be unsuitable for use as a Q-multiplier because of the temperature dependence of the active components. As the operating level increased, the junction temperature would rise, causing the gain to change. Since the system was initially very near oscillation, a minute increase in gain would cause a considerable change in the operating level, thereby leading to a runaway condition.

As stated above, all of these amplifier investigations were based on the assumption that the complete discrepancy between theory and experiment was caused by the amplifier noise and, in particular, that it was not caused by overly optimistic measurements of P_o, μ_{eff}, H_{sig}, etc. Noise sources other than straightforward Johnson noise were also neglected, e.g. tank pulling, skirt noise contributions, etc. It would be very optimistic, then, to expect an improvement even approaching a factor of 3 in sensitivity if the amplifier were replaced with one having perfect noise characteristics.

(d) Information Retrieval: Before it was realized that pulsed operation offered no advantages, one of the foremost engineering problems was that of recovering the information from the output spectrum of the maser.

A considerable amount of effort was expended in investigating suitable systems, and, although the information is now of limited usefulness, the investigations were performed under the contract and, for this reason, a brief description of the accomplishments are recorded here.

The information retrieval system actually used for sensitivity measurements was described in the previous report, RADC-TR-64-567.* Three methods of recovering information from a series of frequency modulated bursts were considered; one was described in the proposal and two others were devised during the course of the program. In the first method, shown in Figure 2-15, the pulsed r.f. signal was fed into a frequency discriminator sufficiently wide band to accept all the important sidebands in the signal spectrum.

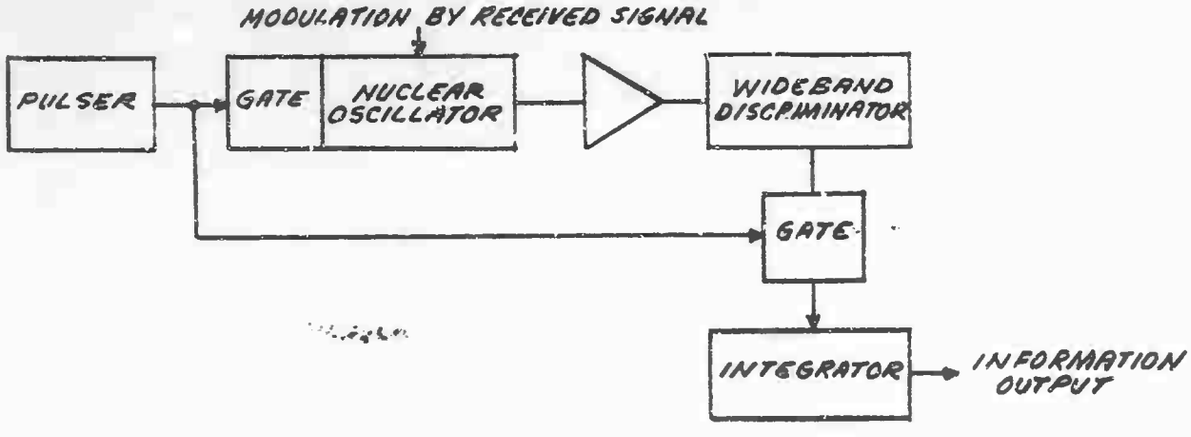

Figure 2-15 - Wideband Discriminator

As the information desired is contained in a great many sub-sidebands surrounding each of the major sidebands, the whole spectrum must be accepted by the discriminator. For discriminator aperture $B_{disc} < \Delta f$, the spectrum width, the output signal-to-noise ratio becomes inadequate.

*AD 619 043

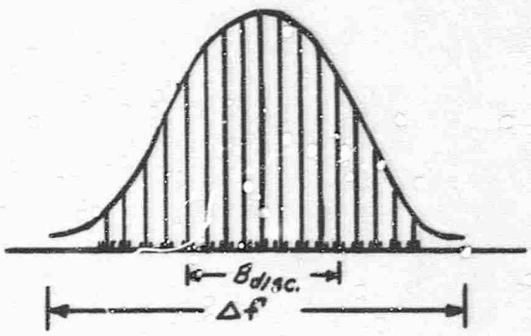

An important consideration in the evaluation of this scheme is that the gate time during which the final integrator accepts information (contained in the stepwise varying output of the discriminator) is extremely short, so that little or no averaging of noise occurs. The essential instantaneous glimpse of signal-to-noise allowed the integrator is held during the whole of the "read out" period between bursts.

A second difficulty also developed. Suppose for the moment that the target sensitivity is 10^{-9} gauss; then with the effective permeability of $\mu_{eff} = 6$, the field in the air gap is 6×10^{-9} gauss, which corresponds to a frequency deviation of

$$\Delta \nu \tilde{=} 2.5 \times 10^{-5} \text{ Hz.}$$

If such a frequency deviation corresponds to a microvolt change out of the discriminator then the whole of the 100 kHz discriminator slope (assuming 10 μsec r.f. bursts) must cover a 4000 volt range. Alternatively, one could build a comb filter that would pick out each major sideband and apply it to its own individual discriminator. There would be required 250 such filter discriminators each with a slope of about .04 volt per Hz deviation.

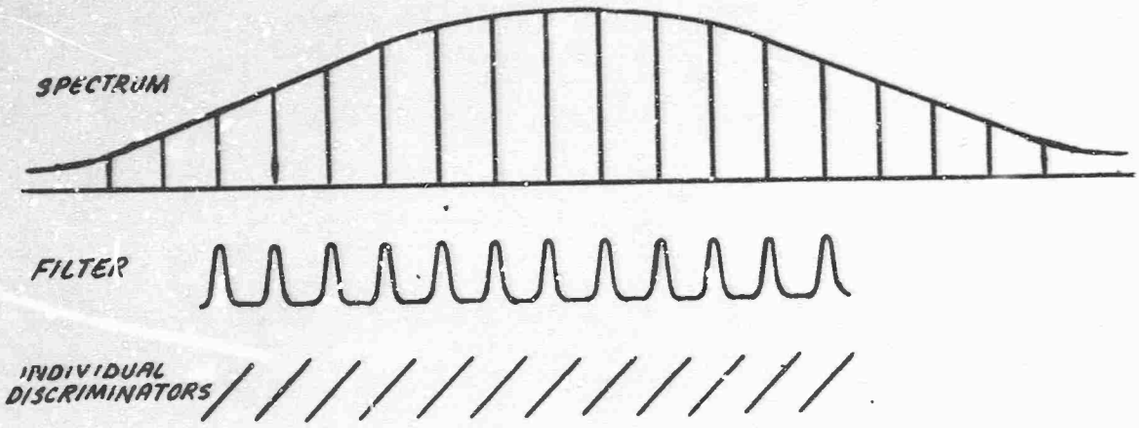

A revised scheme that was introduced is shown in block diagram form in Figure 2-16.

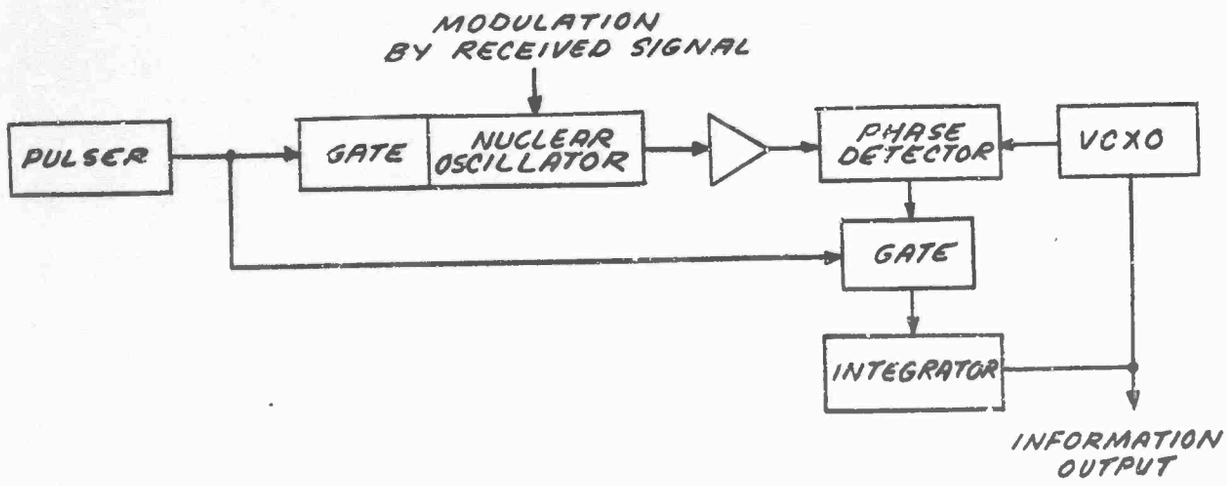

Figure 2-16 - Phase Detector

Letting θ_N be the phase of the nuclear oscillator signal and θ_X be the phase of the VCXO (voltage controlled crystal oscillator) signal, the control voltage V_C out of the phase detector is:

$$V_C = a\,(\theta_N - \theta_X), \text{ where } |\,\theta_N - \theta_X| < \pi\,.$$

If we let a, b, k, k' and α be constants and let the subscripts N and X have the same reference as above, then:

$$\nu_x = 2\pi\dot{\theta}_x = \nu_{x0}(1+bV_c)$$

$$\nu_N = \gamma H_z = \gamma(H_0+\Delta H) = 2\pi\dot{\theta}_N$$

$$\dot{V}_c = \frac{a}{2\pi}(\nu_N - \nu_x)$$

$$\dot{V}_c = \frac{a}{2\pi}\left[\gamma H_0 + \gamma\Delta H - \nu_{x0} - bV_c\nu_{x0}\right]$$

$$\dot{V}_c + \frac{ab\nu_{x0}}{2\pi}V_c = \frac{a}{2\pi}(\gamma H_0 - \nu_{x0} + \gamma\Delta H)$$

Let ν_{x0} be adjusted so that $\nu_{x0} = \gamma H_0$, then:

$$\dot{V}_c + kV_c = k'\Delta H$$

And, ignoring the transient term, we see that V_c can differ from $\alpha\,\Delta H$ at most by the phase; therefore, we may write, ignoring any phase difference (which will be small if ΔH changes only slowly with time),

$$V_c = \alpha\,\Delta H\,.$$

As a function of time, the performance of the control voltage of the phase locked oscillator would be as depicted in Figure 2-17.

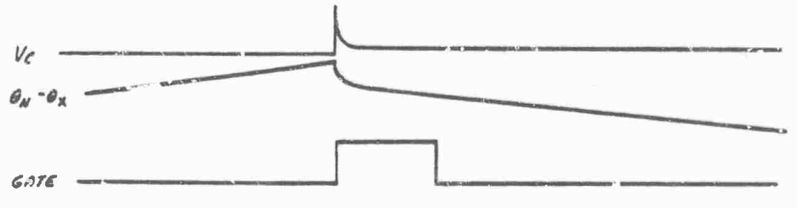

Figure 2-17 - The Phase Locked Oscillator Control Voltage

Two objections to this scheme are that the oscillator may apparently be locked to any one of the major sidebands of the pulsed r.f. spectrum and thus may be presumed to accept information from only one. Therefore, again assuming a sensitivity of 10^{-9} gauss and a μ_{eff} of 6, the phase detector would have to derive its steady state offset from the 1.6×10^{-10} radian/cycle phase advance of the nuclear oscillator. Use of 10^5 times multipliers could be employed to ease the requirements on the phase detector, but then a local oscillator of great stability is required for heterodyning back a lower frequency. The final scheme (see Figure 2-18) avoids the problem of local oscillator stability but still has the drawback that only one major sideband constructively contributes to the output information.

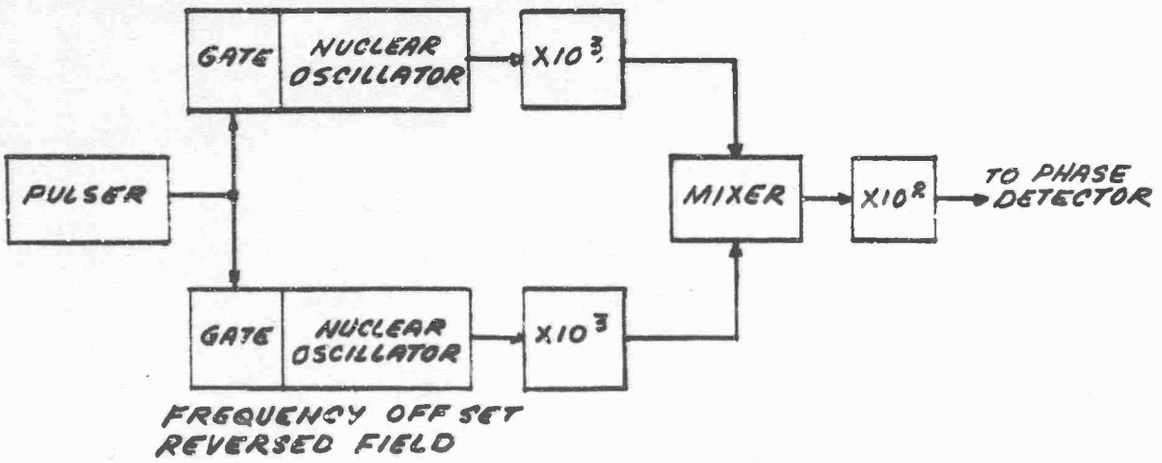

Figure 2-18 - Double Antenna Scheme

Of these several schemes for extracting FM information from such a signal, the most promising seemed to be the multiple segment wide band discriminator. The development of such a device would be a major undertaking in itself and was beyond the scope of the present contract.

(e) Bandwidth: The sensitivity of the proton maser antenna is proportional to the square root of the information bandwidth, and can be improved by using smaller bandwidths. In general, the bandwidth will be determined by the information rate required and will not be subject to change for the purpose of improving the sensitivity.

Since the required bandwidth was specified in the Statement of Work there was no experimental investigation of the possibility of improving the sensitivity by using narrow bandwidths.

(f) Pulsing for Data Handling: Although the pulse method does not give the large increase in rotating magnetization that was originally sought, the possibility that an advantage might be gained by a pulse method through data handling improvement was explored. This possibility was suggested by experiments in NMR spectroscopy which utilize pulse methods for improvement of sensitivity.[8] In these experiments a sequence of repetitive r.f. pulses are applied to the system under investigation, and the response of the system is recorded. By Fourier transforming the integrated time responses, the spectrum is recovered from these data. This method gives a sensitivity improvement over single sweep methods since the entire spectrum is excited simultaneously. To achieve analogous results in the frequency domain, one would require a multichannel spectrometer using several trans-

---

[8] Ernst and Anderson, "Application of Fourier Transform Spectroscopy to Magnetic Resonance", RSI 37, 93 (1966)

mitters and receivers at different frequencies which correspond to different points in the spectrum. While this method is useful where a complicated spectrum is to be investigated, for our situation where only a single frequency is involved, no advantage is gained over using a single narrow filter. In fact, one loses averaging time by the factor of the duty cycle, and hence loses sensitivity. Therefore, in this application, pulsing does not give an advantage from a data handling viewpoint.

2.2 TECHNIQUES FOR PROVIDING VLF TUNING

2.2.1 Introduction

Two methods were considered for providing tuning of the antenna. One, the TRF method, consisted of simply tuning the electronics to pick up the desired sideband of the maser, and the other, the heterodyne method, was analogous to a superheterodyne receiver.

The tuned radio frequency (TRF) method had the disadvantage that the modulation index decreased with increasing carrier frequency, thereby giving decreased sensitivity at the higher frequencies. In fact, increasing the carrier frequency from 100 Hz to 10,000 Hz would degrade the sensitivity by 40 db. This method was rejected because of the poor sensitivity at large frequencies.

The heterodyne method, on the other hand, permitted the reception of the higher frequencies with a sensitivity comparable to that attained for low frequency reception. This feat was accomplished by magnetically chopping the received signal at the "local oscillator" rate, thereby translating it to the fixed frequency f_{IF}. The electronics were then tuned to receive only the maser sidebands corresponding to f_{IF}, and tuning was accomplished by varying the "local oscillator" frequency.

The magnetic field at the sample resulting from the received signal was chopped by changing the effective permeability of the magnetic structure at the local oscillator rate. The mathematical demonstration that this technique produces the desired results - a magnetic field varying with the frequency f_{IF} at the sample - is quite simple. The received signal may be expressed as:

$$H_{rec}(t) = H_r \cos\left(\frac{f_r}{2\pi} t\right) .$$

Let us assume that the effective permeability of the magnet structure, $\mu_{eff}(t)$, is being varied so that the fundamental component is at the frequency f_{LO}, and that the form of $\mu_{eff}(t)$ is:

$$\mu_{eff}(t) = \mu_o a_o + \mu_o a_1 \cos\left(\frac{f_{LO}}{2\pi} t\right) + \mu_o \sum_{n=2}^{\infty} a_n \cos\left(\frac{n f_{LO}}{2\pi} t\right)$$

If we also assume that f_{LO} and f_{IF} are chosen so that there will be no interference from components at frequencies $2f_{LO} - f_r$, $3f_{LO} - f_r$, etc., then we can let $\mu_{eff}(t)$ be written in the form:

$$\mu_{eff}(t) = \mu_o \left[a_o + a_1 \cos\left(\frac{f_{LO}}{2\pi} t\right)\right].$$

The time dependent magnetic field at the sample is given by:

$$H_{sample}(t) = \frac{\mu_{eff}(t)}{\mu_o} H_{rec}(t)$$

so that

$$H_s(t) = H_r \left[a_o + a_1 \cos\left(\frac{f_{LO}}{2\pi} t\right)\right] \cos\left(\frac{f_r}{2\pi} t\right)$$

or,

$$H_s(t) = a_o H_r \cos\left(\frac{f_r}{2\pi} t\right) + a_1 H_r \cos\left(\frac{f_{LO}}{2\pi} t\right) \cos\left(\frac{f_r}{2\pi} t\right)$$

giving:

$$H_s(t) = a_o H_r \cos\left(\frac{f_r}{2\pi} t\right) + \frac{a_1 H_r}{2}\left[\cos\left(\frac{f_r + f_{LO}}{2\pi} t\right) + \cos\left(\frac{f_r - f_{LO}}{2\pi} t\right)\right]$$

The term oscillating at the sum frequency does not interest us since it will not be detected by the electronics, therefore we may write:

$$H_s(t) = a_o H_r \cos\left(\frac{f_r}{2\pi} t\right) + \frac{a_1}{2} H_r \cos\left(\frac{f_{IF}}{2\pi} t\right),$$

where it is assumed that f_{LO} has been adjusted so that $f_r - f_{LO} = f_{IF}$. This is just the result we wished to demonstrate. The associated waveforms for an idealized case in which μ_{eff} is switched on and off are shown in Figure 2-19.

Since the effective permeability cannot be less than zero and since it cannot exceed the maximum CW value $(\mu_{eff})_{max}$, we can conclude that:

$$a_o + a_1 = (\mu_{eff})_{max},$$

where any non-sinusoidal characteristics of $\mu_{eff}(t) - \mu_o a_o$ have been neglected. Therefore, the practical problem reduces to making $a_1 - a_o$ as small as possible. The various methods considered for accomplishing this task are reported in the following subsections.

2.2.2 Mechanical Methods

The mechanical method of producing the time variation of the effective permeability required some means for periodically opening and closing a gap in the flux concentrator rods. This requirement suggested the possibility of rotating a section of the flux concentrator rod as shown in Figure 2-20.

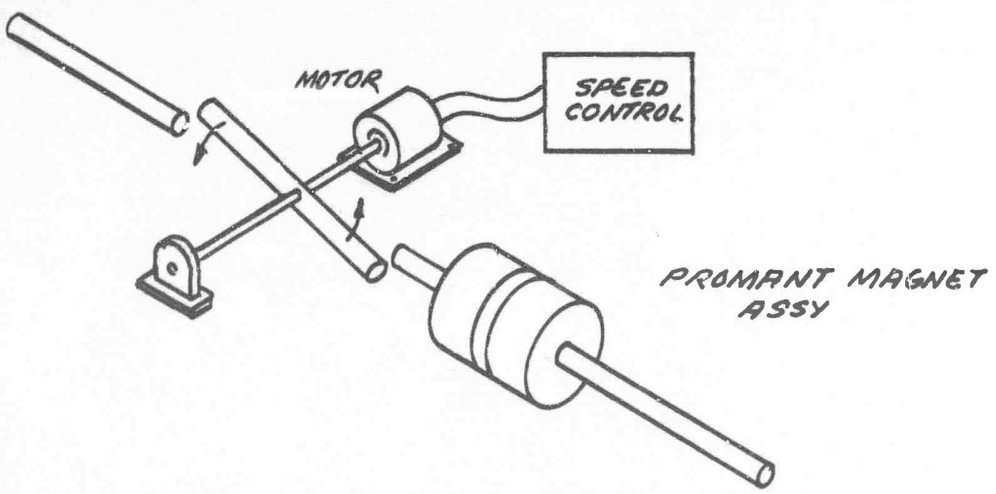

Figure 2-20 - Principle of the Mechanical Method

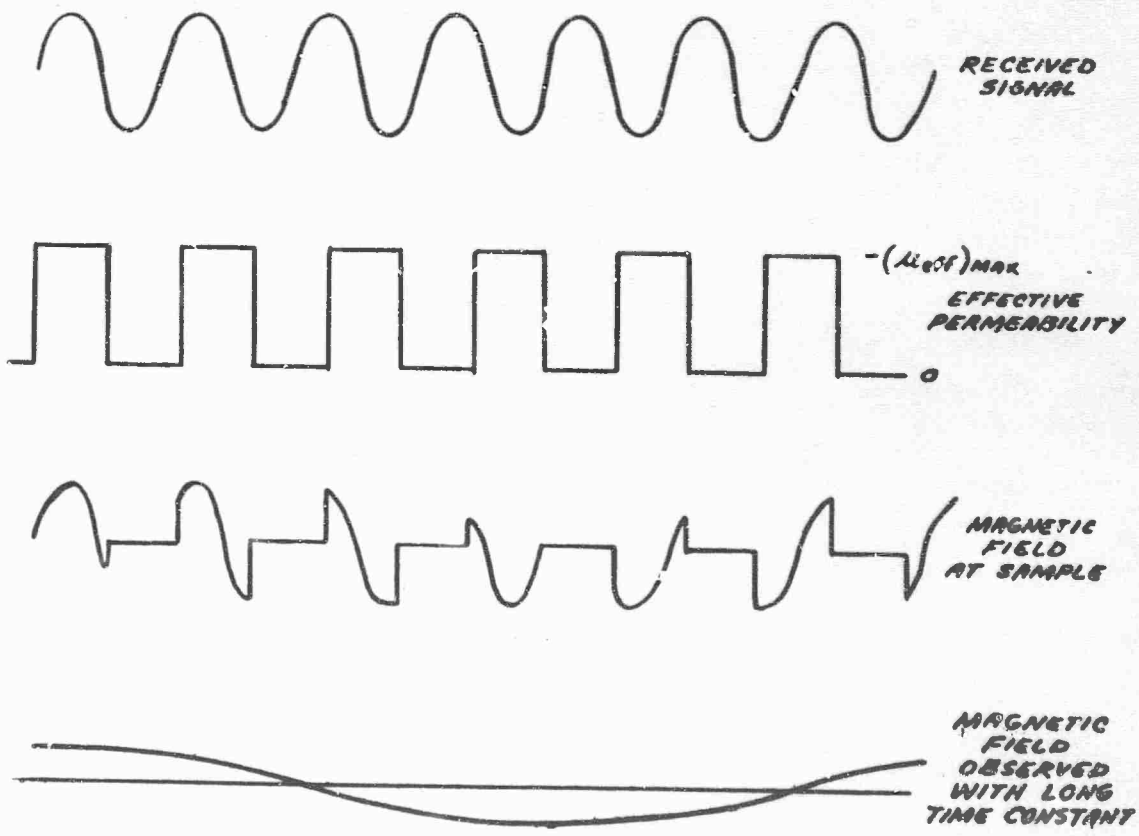

Figure 2-19 - Waveforms Associated with Magnetic Heterodyning

An experiment was performed with just such an arrangement and, although an effect was observed, the results were not encouraging. Next, a pair of pieces (one for each arm of the flux concentrators), as shown in Figure 2-21, were constructed to replace the rotating rod. The performance was somewhat improved; however, mechanical methods were abandoned when it was found that electronic techniques offered promise.

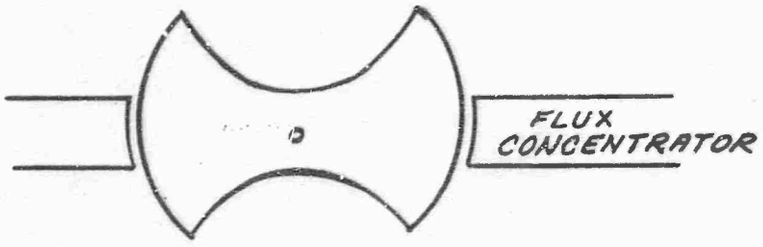

Figure 2-21 - Improved Mechanical Chopper

The mechanical method had the severe disadvantage that extremely high rotation rates would be required for the higher carrier frequencies. For instance, a rotation rate of 60,000 rpm would be required to receive a 1,100 Hz signal. Such rotation rates are not generally considered possible.

2.2.3 Saturation Methods

A method of μ-switching which depended on saturating a portion of the flux concentrator rods periodically was considered briefly; however, it was soon abandoned when the difficulties were fully appreciated. A schematic diagram illustrating this method is shown in Figure 2-22. One of the problems results from the large unwanted time varying magnetic field produced at the sample by this method. This field can be greatly reduced by opposing the two saturating coils; however, perfect balance cannot be attained, and

the residual modulated field is still far too big.

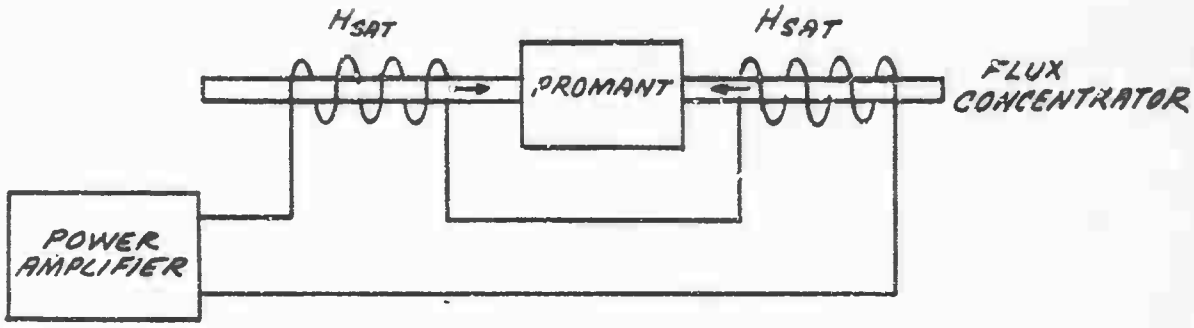

Figure 2-22 - Saturation Method

A fantastic amount of power is required to operate the saturation coils at high frequencies. A rather large volume of the magnetic material must be carried around the hysteresis loop many times per second (depending on the carrier frequency) resulting in a large power loss.

The third, and most severe, problem is the difficulty of causing any change in μ_{eff} by saturating μ. The normal value obtained for μ_{eff} was 6. For the heterodyning to be at all practical, μ_{eff} would have to be reduced to less than one-half of its original value. Recall that the formula for μ_{eff} is:

$$\frac{1}{\mu_{eff}} = \frac{1}{\mu} + \frac{N}{4\pi} \quad ,$$

where μ is the permeability of the rods, and $\frac{N}{4\pi}$ is the demagnetization. Since μ is extremely large, $\frac{1}{\mu}$ can be neglected; therefore,

$$\frac{N}{4\pi} = \frac{1}{6}$$

$$N \simeq 2 \, .$$

The arbitrary requirement above that $a_o - a_1 \leq \frac{1}{2}(a_o + a_1)$ or $a_o < 3a_1$ means that the saturated value of μ indicated by μ_{sat} must obey the following equation:

$$\frac{2}{(\mu_{eff})_{max}} \leq \frac{1}{\mu_{sat}} + \frac{N}{4\pi}$$

or, for the actual parameters of the apparatus,

$$\frac{1}{3} \leq \frac{1}{\mu_{sat}} + \frac{1}{6} .$$

Therefore,

$$\mu_{sat} \leq 6 .$$

A special material, Carpenter High Permeability "49" Alloy, which saturates at an extremely small field (about $H_{sat} = 0.05$ Oe, for which $B \simeq 10{,}000$ gauss) was used in the experimental tests of this method. By extrapolating the manufacturer's graphs, it is estimated that the H field required to reduce the permeability to $\mu = 6$ is approximately 3000 Oe. The production of such a field would require a coil of many turns and many amperes of current.

This method was dismissed as impractical.

2.2.4 Eddy Current Methods.

The method by which success was achieved was the eddy current flux-cancelling method. Two eddy current coils were wound around the flux concentrators as shown in Figure 2-23. The operation of this method is based on the exclusion of time varying flux from a shorted turn(s), i.e., the emf induced in a shorted coil gives rise to an eddy current which, in turn, produces a flux which tends to cancel the applied flux (Lenz's law). Clearly, the resistance around the loop of the coil plus its "short" must be kept at a minimum for this method to be effective and, in fact, finding a "switch" with sufficiently low resistance was the most difficult practical problem associated with the method.

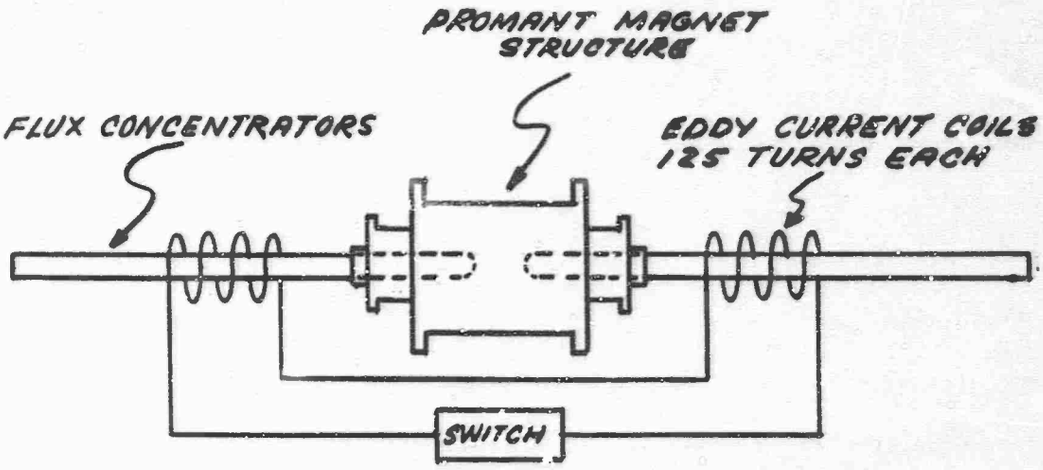

Figure 2-23 - Promant with Eddy Current Coils

Tests were performed to determine the possible effectiveness of the method. Measurements were made with both the Promant assembly itself (Figure 2-23) and with a special test structure made by removing the flux concentrators from Promant and applying them directly to a test coil as shown in Figure 2-24.

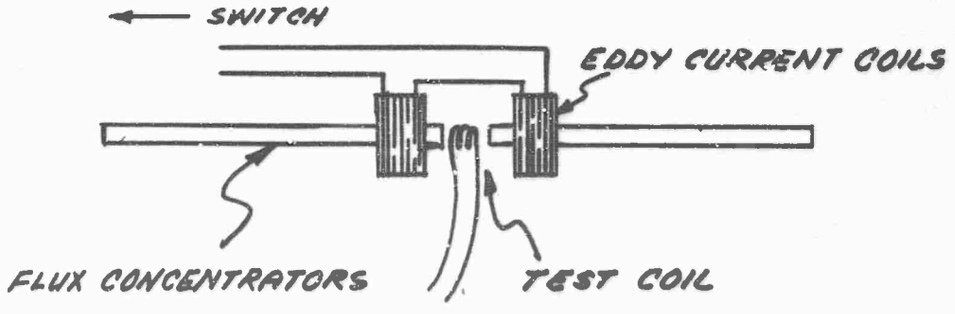

Figure 2-24 - Test Structure

The results obtained are as follows:

Set-Up	Figure	Effective Permeability (1 kc signal) Switch Open	Switch Closed
Promant	2-23	6	3.2
Test Structure	2-24	30	1

The values shown here were obtained under the conditions described in the following paragraph.

It was found that the change that could be produced in the effective permeability depended strongly on the proximity of the eddy current flux-cancelling coils to the gap. As an illustration of this effect, it was observed using the test structure that the effective permeability (which was 30 for the switch-open condition) could be reduced to 1 if the coils were as near the gap as possible, whereas the effective permeability could only be reduced to 10 if the coils were 25 cm from the gap. The numbers given in the table above were obtained with the Promant eddy current coils pushed tightly against the magnet structure. Since the Promant magnet without the laminated flux concentrators (but with the copper dynamic flux concentrators) had a non-programmable effective permeability of $\mu_{eff} = 2.2$, and since about 9 inches of each magnetic flux concentrator lay on the gap side of its eddy current coil, the data is self-consistent.

As stated above, finding a switch that could operate at up to 10,000 Hz and yet have extremely low "on" resistance posed quite a problem. The solution finally obtained is shown schematically in Figure 2-25. The diodes were chosen for minimum potential developed between points A and B, which proved to be an unexpectedly difficult selection. The results of using this

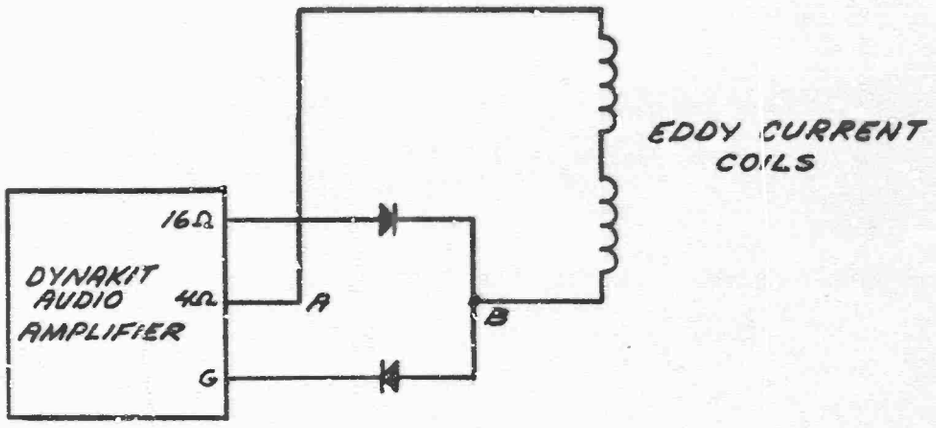

Figure 2-25 - Dynamic Switch

dynamic switch were particularly encouraging and the design was considered quite successful.

All of these features found desirable were applied to the modified Promant as described in Section 3. Tests were made to determine the success of the tuning method. The results showed that this was very successful (see Figure 3-8). The sensitivity at 10 kHz was improved by nearly 30 db, and the sensitivity was relatively constant over the whole upper frequency range.

A further improvement in performance may be obtained by gating the electronics so that the maser is only observed during the switch-open portion of each cycle. Only noise would be expected from the maser during the switch-on portion of the cycle. Another possible source of improvement would be a redesign locating the eddy current coils nearer the air gap.

SECTION 3

MODIFICATIONS

3.1 MODIFICATIONS TO THE PROMANT MAGNET

3.1.1 Dynamic Flux Concentrators

The promant magnet was dissasembled and two copper Flux concentrator plates were secured to the soft ferrite pole pieces with double sided sticky Scotch tape #410. The geometry of the plates is shown in Figure 3-1.

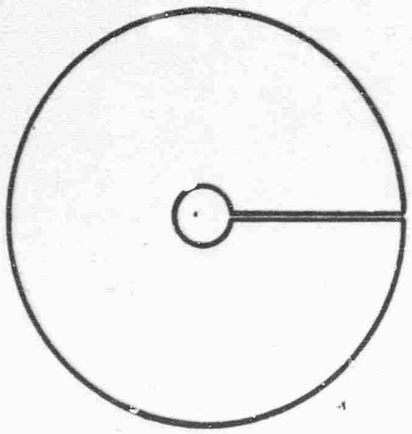

Figure 3-1 - Dynamic Flux Concentrators

The performance of the plates in air is given in the following table.

Frequency	Effective Permeability
0	1
100 Hz	1.9
1,000 Hz	2.5
10,000 Hz	2.3

The effectiveness of the plates in concentrating the AC flux in the air gap is strikingly seen in Figures 3-2 and 3-3. Figure 3-2 was made* before the concentrator plates were inserted and shows a barely discernable reduction of the AC flux near the outer edges of the pole plates. In contrast note the pattern with the plates in Figure 3-3 which shows a very high degree of concentration in the central region of the poles. The enhancement of the effective permeability of the promant magnet obtained with the use of these plates was slightly less than would be expected on the basis of their performance in air. This discrepancy resulted from the fact that the change in the geometry of the AC air gap increased the demagnetization factor for the two magnetic flux concentrator rods. The final effective permeability for the promant magnet obtained by this and all other techniques combined is shown in Figure 3-4.

3.1.2 Flux Concentrator Extention

The flux concentrator length was extended by 13%, bringing the total length per side to 37.5". The extentions were two 4.5" long sections of 1.5" diameter iron pipe, slit along a element of the side to prevent eddy currents.

The final effective permeability of promant is shown in Figure 3-4.

3.1.3 Flux Concentrator Bias Magnets

It was observed that the flux concentrators could be moved closer to the back of the soft ferrite pole pieces without impossibly damaging the air-gap field homogenity if small bias magnets were placed on the ends

---

*A word is in order concerning the techniques used to plot Figure 3-2 and Figure 3-3. A modified drafting machine having an NMR coil attached to one extremity and a marker attached to the other was used to draw curves of equal magnetic strength, i.e. the NMR coil was moved about in the promant magnet gap along those paths that gave no change in the resonant frequency - the marker then traced out an image of the field contour on a piece of paper.

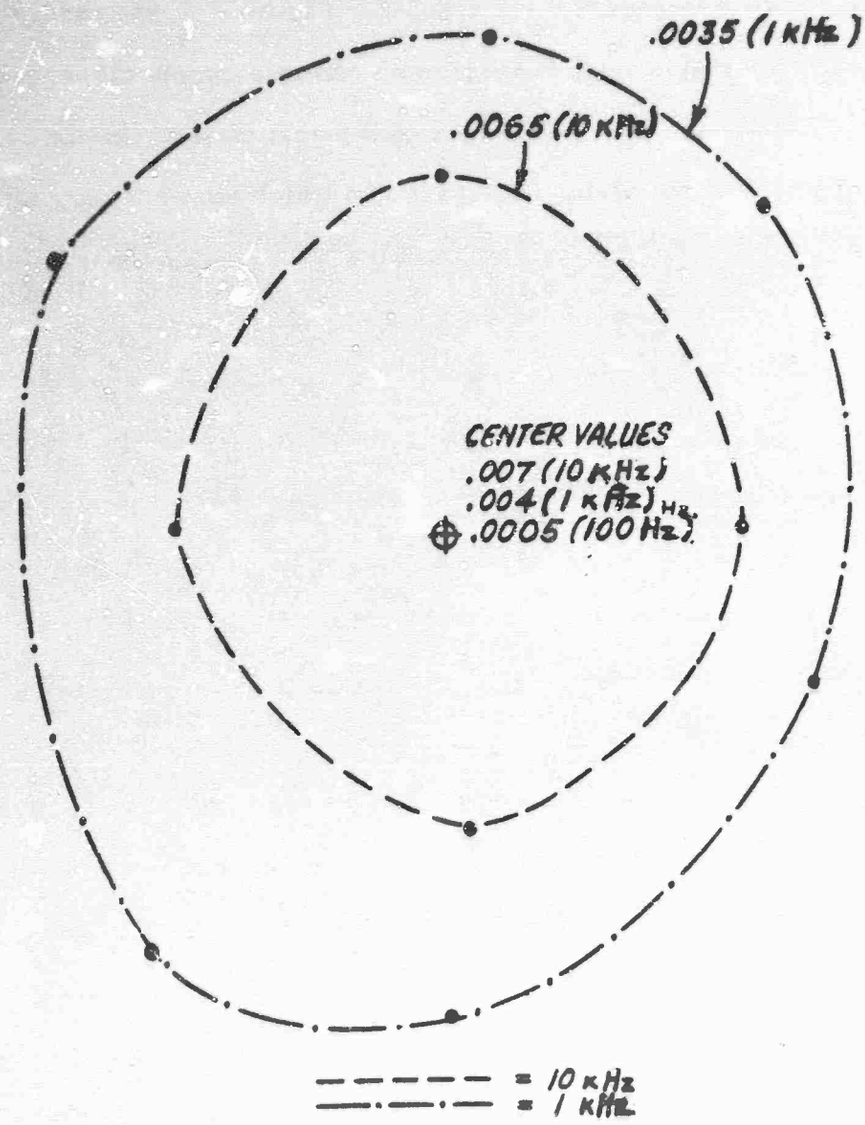

NOTES:

NO OBSERVED CHANGE OVER POLE FACE FOR 100 Hz.

NUMBERS INDICATE RELATIVE FIELD STRENGTH AT FREQUENCY INDICATED.

Figure 3-2 - AC Field Distribution in Magnet Gap without Dynamic Flux Concentrators (Shown Full Scale)

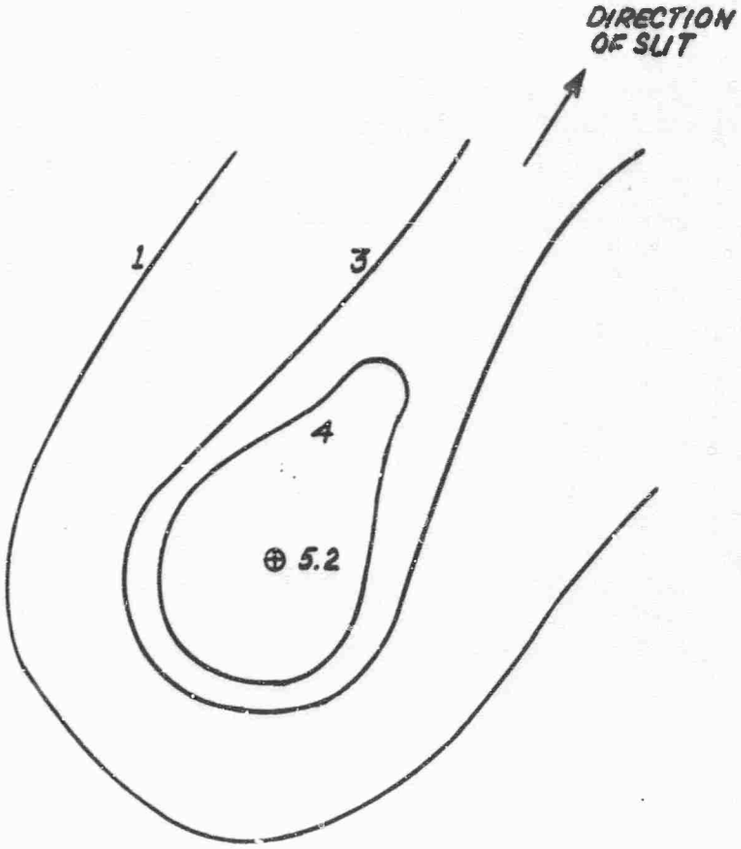

NOTES:

NUMBERS INDICATE RELATIVE FIELD STRENGTH (FREQUENCY = 100 Hz.

FIELD STRENGTH = 3.2 AT CENTER WITHOUT CONCENTRATORS

Figure 3-3 - AC Field Distribution in Air Gap with Dynamic Flux Concentrators (Shown Full Scale)

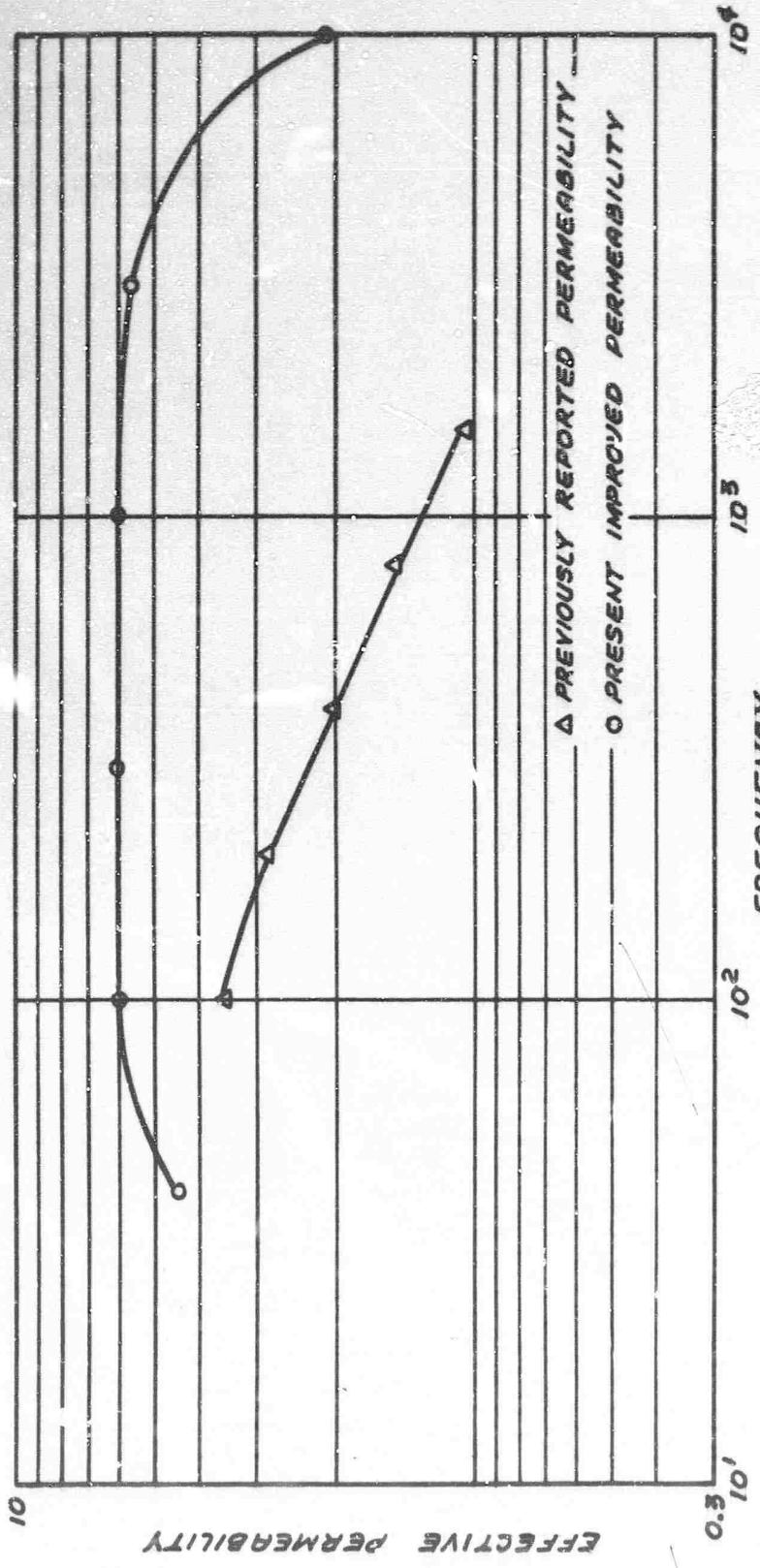

Figure 3-4 - Effective Permeability of Promant Magnet

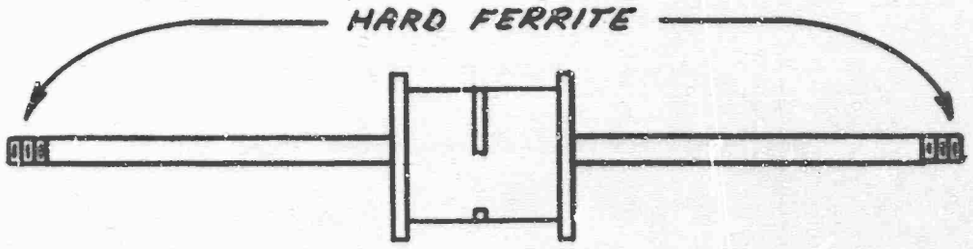

Figure 3-5 - Flux Concentrator Bias Magnets

of the flux concentrator rods as shown in Figure 3-5. This addition does not increase the effective length of the flux concentrators because the intrinsic permeability of hard ferrite is unity. Using this technique, a reasonable homogenity was obtained in the vicinity of the nuclear resonance probe. As determined from Figure 3-6 an inhomogenity in the magnet center of $\epsilon = 4 \times 10^{-5}$ was obtained by using both current shims and the flux concentrator bias magnets.

3.1.4 DC Flux Returns

Because the Promant Magnet had a magnetic field temperature coefficient* of 1.2 gauss/°C. A one degree Centigrade temperature change in the experimental area could move the magnetic field beyond the range of the manual field adjust coil on the control rack. To give a wider range of control, a course field adjustment was provided on the promant magnet. This adjustment consists of a set of flux return bars as shown in Figure 3-7.

*See the previous report RADC-TR-64-567, p. 52.

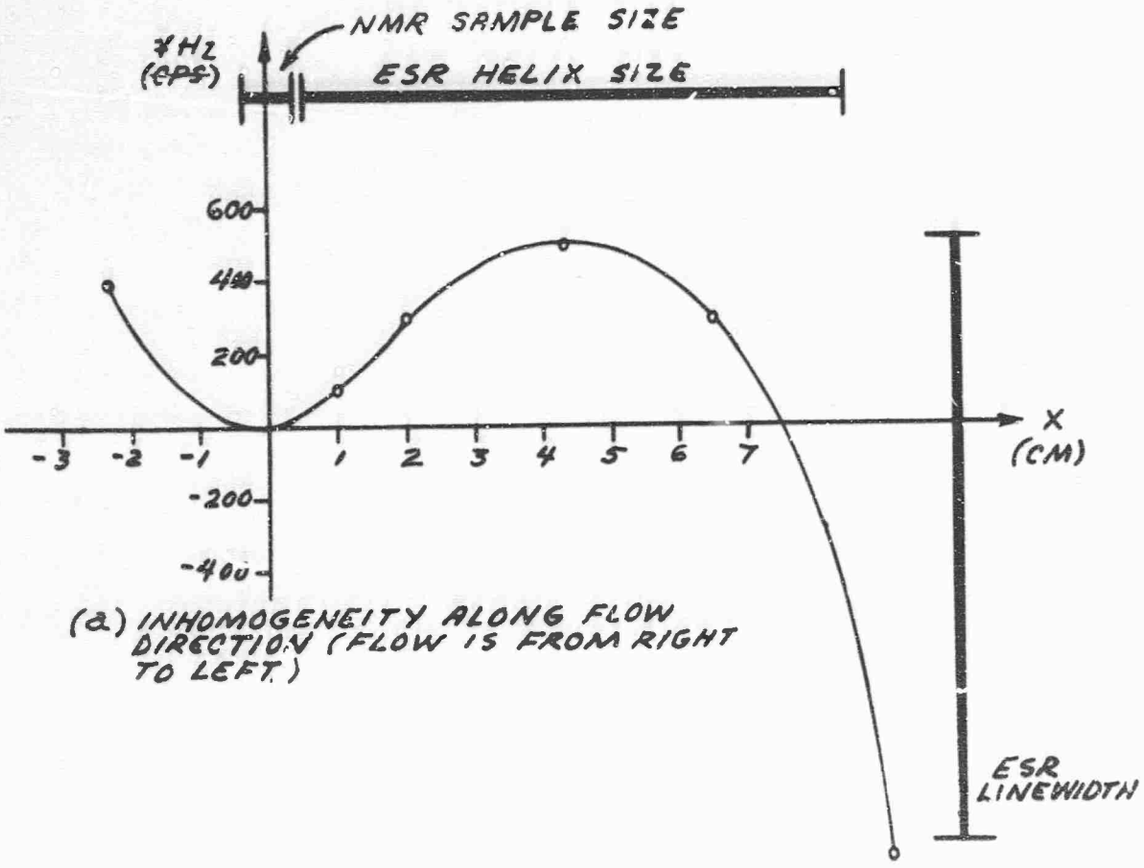

(a) INHOMOGENEITY ALONG FLOW DIRECTION (FLOW IS FROM RIGHT TO LEFT)

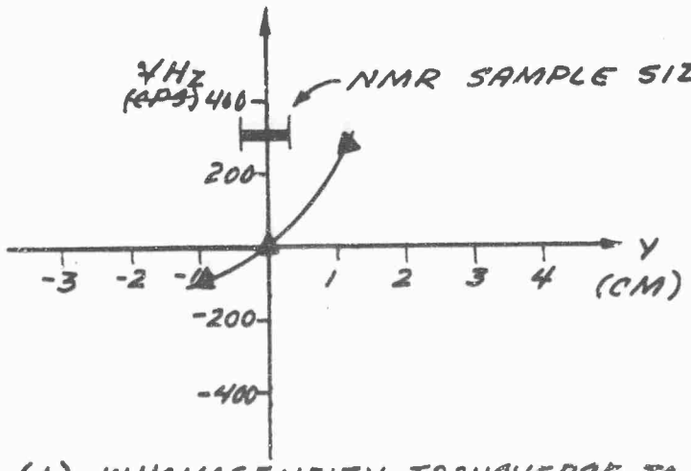

(b) INHOMOGENEITY TRANSVERSE TO FLOW DIRECTION

Figure 3-6 - Magnet Field of Promant Magnet, Frequency Terms

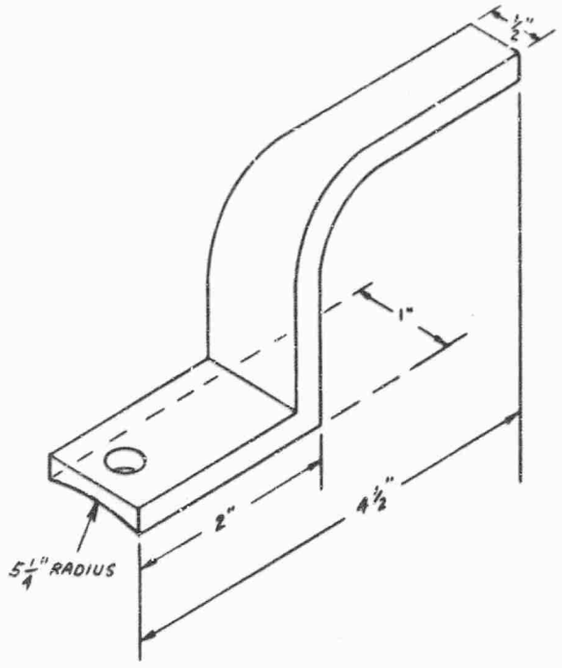

Figure 3-7 - Flux Return Bars

These bars, when mounted at opposite ends of the promant magnet barrel over the backing plates of the bias magnet assemblies were separated by a

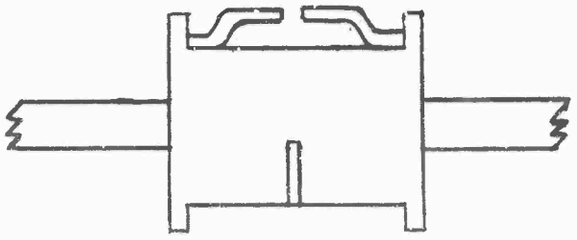

small air gap. This gap could be shunted with iron strips of various thickness giving a small, variable flux return path for the main bias magnets and thereby providing a coarse field adjustment. The most important inhomogenity resulting in the air gap from the installation of the flux return structure was $\frac{\partial H_z}{\partial y}$. This inhomogenity was sufficiently small that it could be compensated with the electrical shim coils.

The flux return bars were used to make changes of the order of 1 gauss in the magnetic field representing a relative change of 0.5%. Even if .5% of the AC flux were lost through the flux return bars it would not be significant.

3.1.5 Eddy Current Windings

To provide for VLF tuning by permeability switching the magnet, about 125 turns of #12 copper wire were wound around the flux concentrator rods just outside the magnet yoke bushing. When shorted these windings partly cancelled the flux passing down the concentrator rods as described in Section 2.2.4. Although these eddy current windings would have been more effective if placed closer to the poll faces, the drastic modification of the magnet that would have been necessary was outside the scope of the contract. The coils as wound had a measured inductance of 7.2×10^{-3} henry when installed on their respective flux concentrators. The reactance at 1 kHz therefore was 45Ω, and, as the ohmic resistance was about 2Ω, the coils were highly inductive.

When located outside the yoke bushings of the promant magnet the shorted eddy current coils could reduce the promant permeability from 6 to 3.2.

The electronic switch described in Section 2.2.4 was also used in the modified Promant.

The sensitivity of the modified apparatus was measured over the higher frequency range and is shown in Figure 3-8. Here the sensitivity is compared with that obtained without the magnetic heterodyning. The improvement is remarkable.

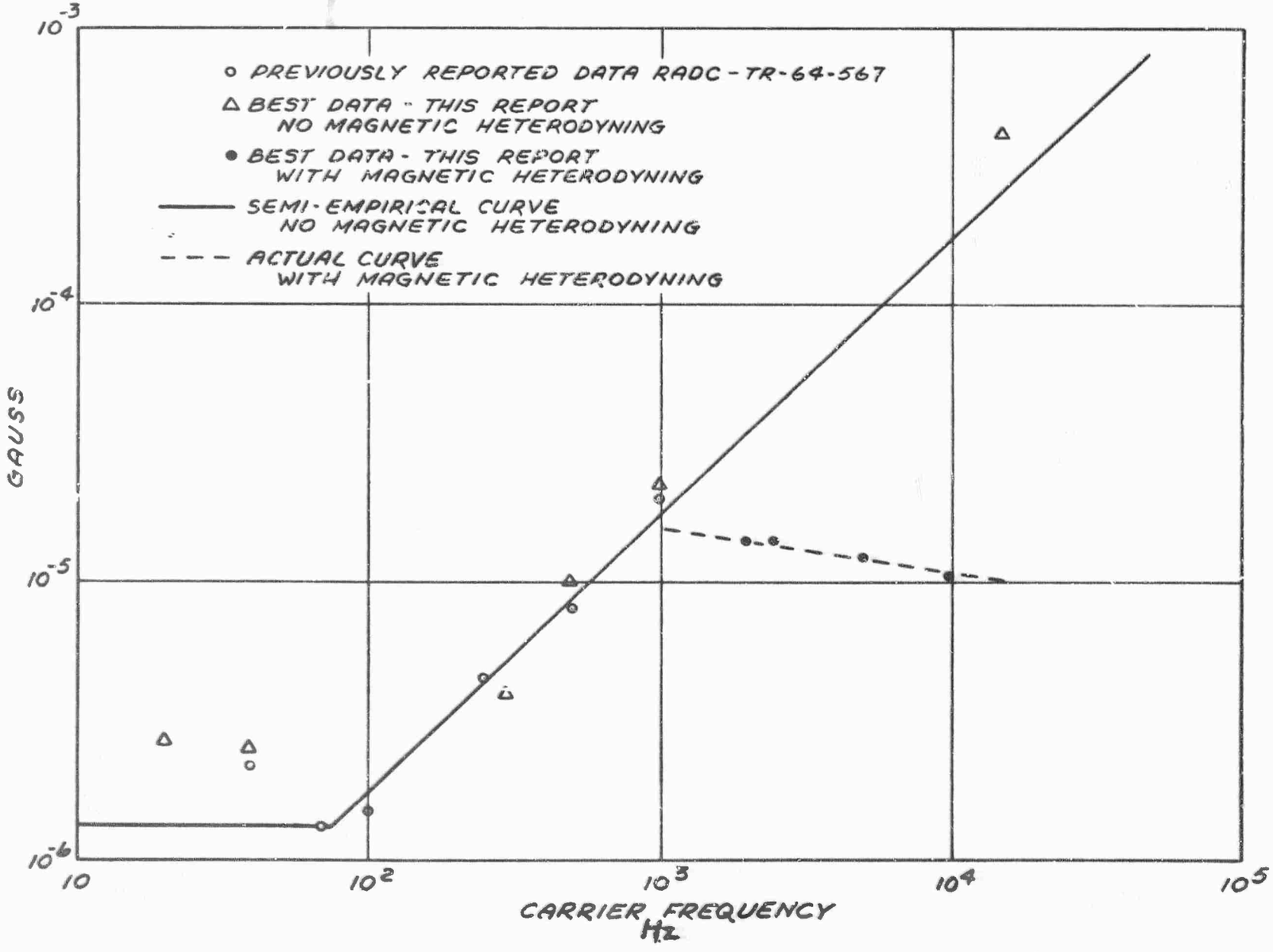

Figure 3-8 - Magnetic Field for S/N = 1 vs Frequency (B = 2.5 Hz)

3.2 NUCLEAR OSCILLATOR ELECTRONICS

3.2.1 NMR RF Bridges

In order to use 10 μsec bursts with an RF bridge for nuclear resonance the bridge must have two essential properties: (1) all circuitry must be at least of 100 kHz bandwidth and (2) the balance must be preserved over the complete bandwidth so that the fourier components of the RF burst will not couple through with greater amplitude than the inbalance component produced by the resonance itself. Much work went into the making of an RF bridge that was at all capable of being used with RF bursts. Only towards the end of the contract was a bridge developed that came close to filling the requirements. Even then the final bridge performed well only with two dummy coils. The best decoupling achieved was -80 db over about a 50 kHz range.

Three bridge designs that were discarded after construction and testing of prototypes are shown in Figure 3-9.

A schematic diagram of the final design which more nearly filled the requirements than any other is shown in Figure 3-10.

Because of the downfall of the pulsing scheme, none of these bridges were incorporated into the Promant device itself; however, the final design was used to obtain the experimental data presented in Section 2.1.3.

3.2.2 Coil Box

A revised coil box was constructed. The new coil box followed the design of the first one except that larger sample volumes were contained in both the helix and the NMR coil, and the NMR coil chamber was made large enough to accept the experimental crossed coil structure had that arrangement been desired.

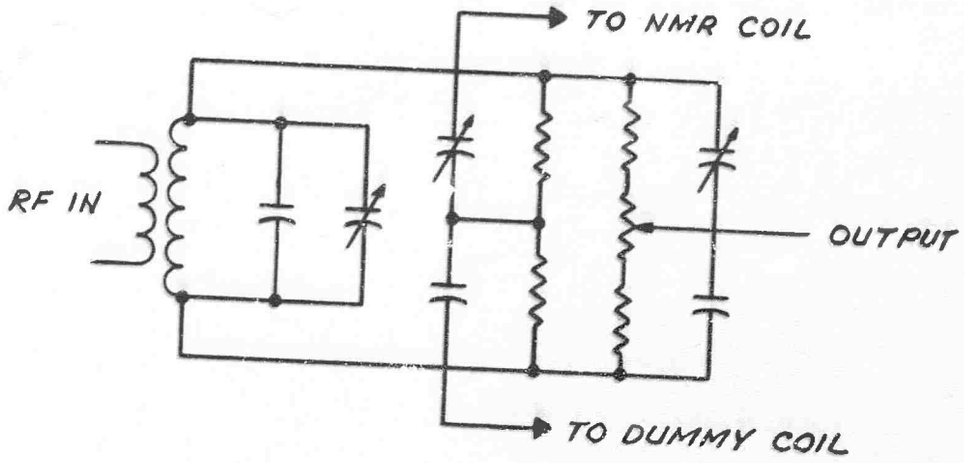

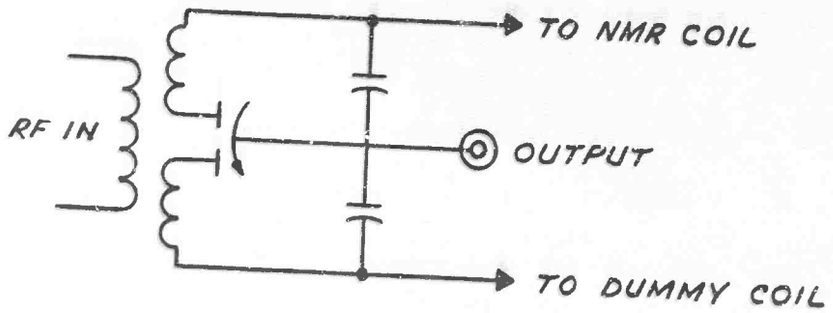

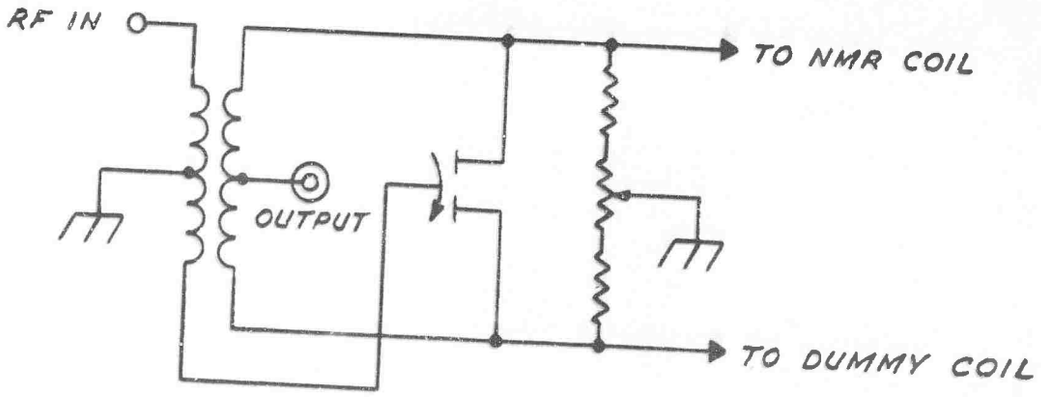

Figure 3-9 - Various Bridge Designs That Were Constructed

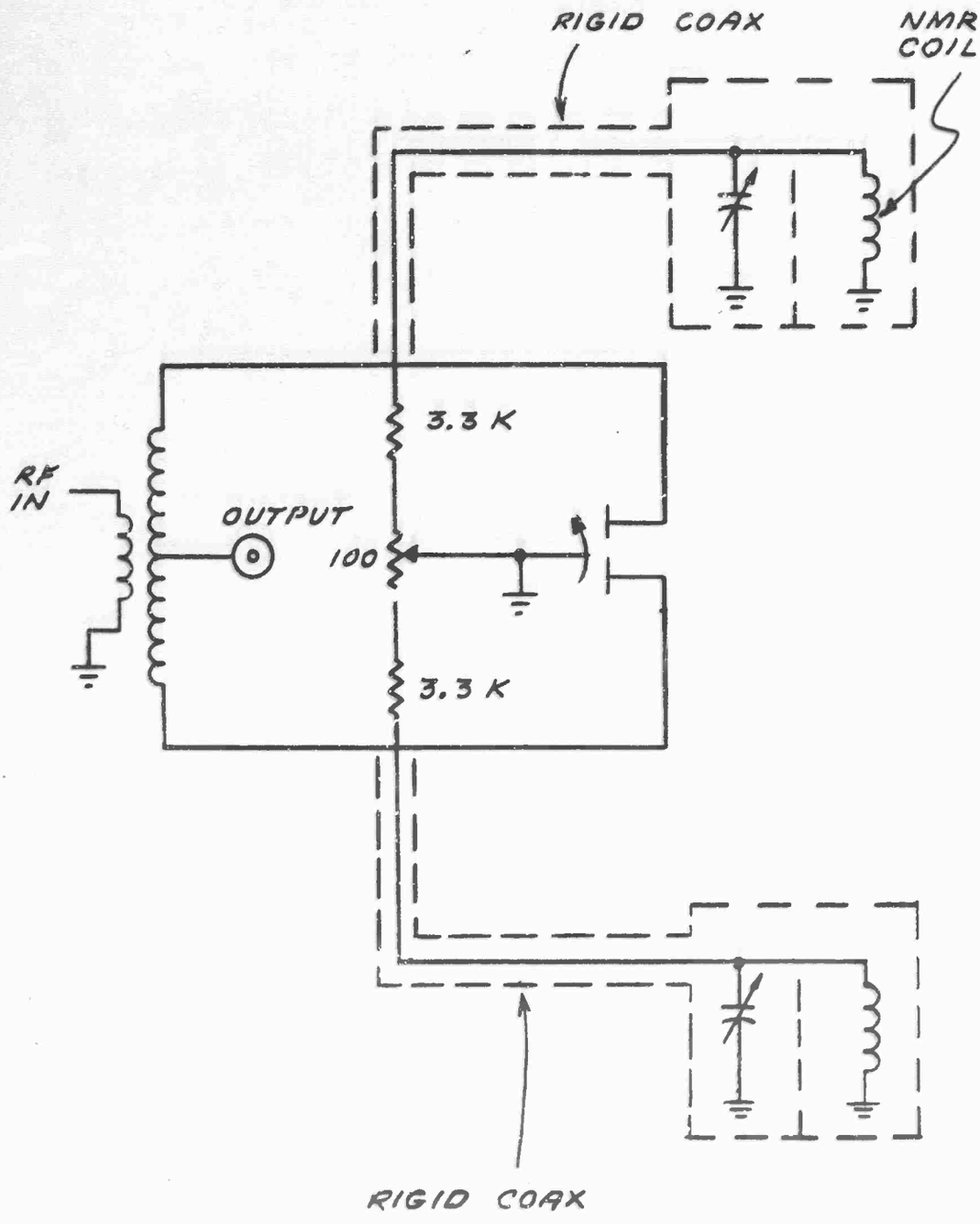

Figure 3-10 - Final Design of the NMR Bridge

The volume of sample in the helix was increased to 3.9 cm^3 so that with the normal flow rate of about 3 cm^3 of liquid/sec., at least 2 proton relaxation would be spent by the sample in the helix. Over the useful life of the sample the proton relaxation times varied from .3 to .5 seconds.

The resulting helix diameter of 1.1 cm mean that to obtain a saturating UHF field to excite the electrons 4 watts of power at 660 MHz were required. (A tunable power oscillator was obtained that could provide this power.) Overhauser effects of at least A = -75 were obtained by this means.

The NMR coil volume was increased by 50% becoming .75 cm long. This change increases the exposure time of the sample to the RF field and thus reduces the line broadening by flow; however, as the sample occupies more space, the magnet must be improved or ϵ the fractional inhomogenity becomes worse (larger). We deduce from plots of the Promant S/N v. s. magnet frequency plots that the operational line width was 40 Hz. A number in keeping with the field spread over the sample is shown in Figure 3-6.

3.2.3 Crossed Coil

A substantial effort was directed toward developing a crossed coil structure with adequate decoupling and sufficient bandwidth to fill the needs of the proposed pulsed nuclear spin oscillator. The experimental crossed coil structure was wound on a form that could be inserted into the NMR coil compartment of the new Promant coil box. The direct linkage flux was controlled by a pair of Bloch paddles. The capacitive coupling was cancelled by a variation of Weavers U-mode* control (see Figure 3-11).

*E.R. Andrew, Nuclear Magnetic Resonance, Cambridge 1958, p. 61.

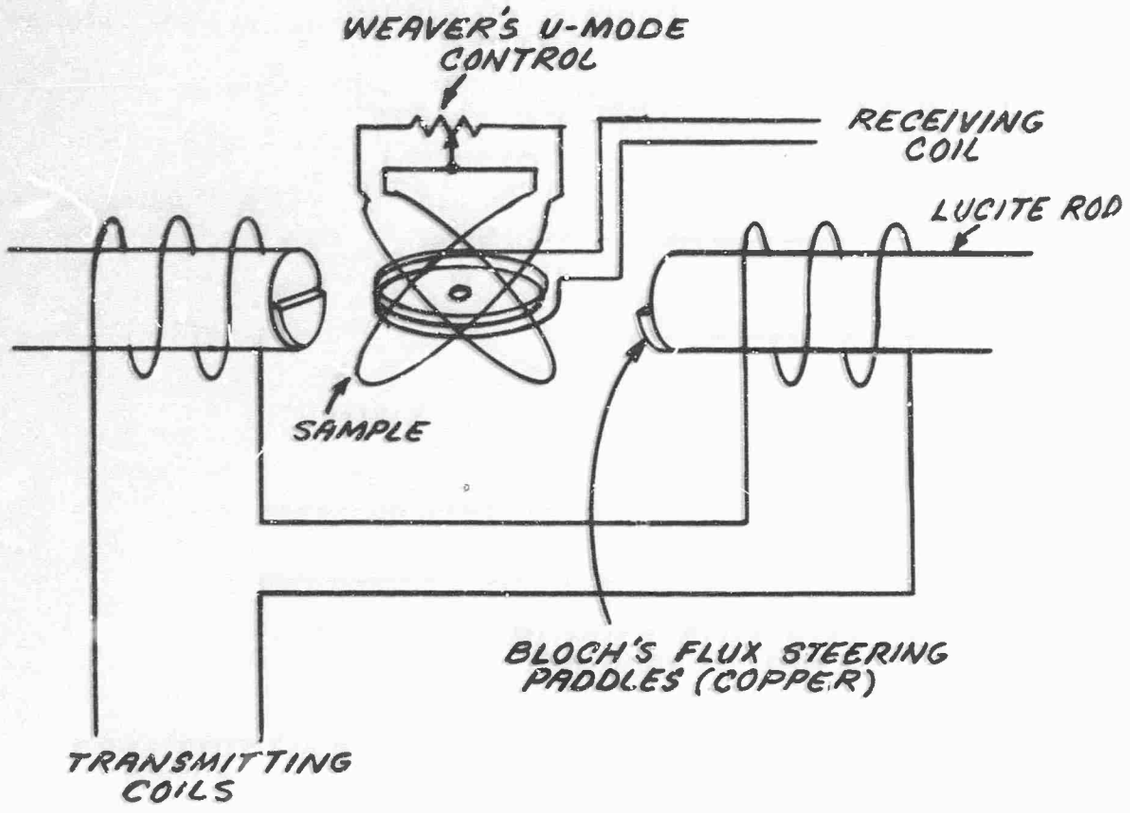

Figure 3-11 - Crossed Coil Showing Bloch's Flux-steering Paddles and an Adaptation of Weaver's U-Mode Control

The maximum decoupling was about -100 db but the feedthrough came up very fast, being intolerably high 10 kHz away from the balance point. It was interesting to note that when the frequency was shifted from design center it was the direct linkage flux that gave the feedthrough problem. This situation prevailed even when the Bloch paddles were removed and the structure was suspended several inches away from metal surfaces.

3.2.4 Sweep Frequency Oscillator

A sweep frequency oscillator was constructed to aid in designing the RF Bridg It was patterned after the VCXO, except that the unit was capable of sweeping over a 100 kHz range. The AGC stabilized oscillator is capable of a maximum undistorted signal of 2.2 volts into the RF bridge

input. The unit swept from 947 kHz to 1057 kHz for a control voltage variation from 6 volts to 2 volts. The schematic is shown in Figure 3-12.

3.2.5 The Q Multiplier

A Q multiplier circuit was constructed using low noise FET's (field effect transistors). With special circuitry to cancel the self heating of the transistors the circuit will Q multiply by a factor of about 800 before breaking into oscillation.

This performance was not sufficiently useful to justify replacing the original Q multiplier. Refer also to Section 2.1.2 where the Q multiplier problems were discussed in greater detail.

3.2.6 Null Amplifier

A null amplifier was constructed to amplify the resonance signal at the output of the bridge or crossed coil. The amplifier had a maximum gain of 68.8 db and a maximum undistorted output of 550 mv pp into a 15Ω impedance. The equivalent noise input is 10 uv pp. In use the amplifier was powered with batteries. The frequency response is given in the following table.

Frequency	500 kHz	600	800	1000	1200	1500
Variation	+1.4 db	+1.6	+1.0 db	0	-1 db	-2.5

The schematic diagram is shown in Figure 3-13.

3.3 DATA RECOVERY ELECTRONICS

Of the data recovery electronics described in Section 2.1.4(d) only the voltage controlled crystal oscillator was actually built. The problem of building the orthogonal coupler and verifying the performance of the pulsed spin system had a priority claim to man hours.

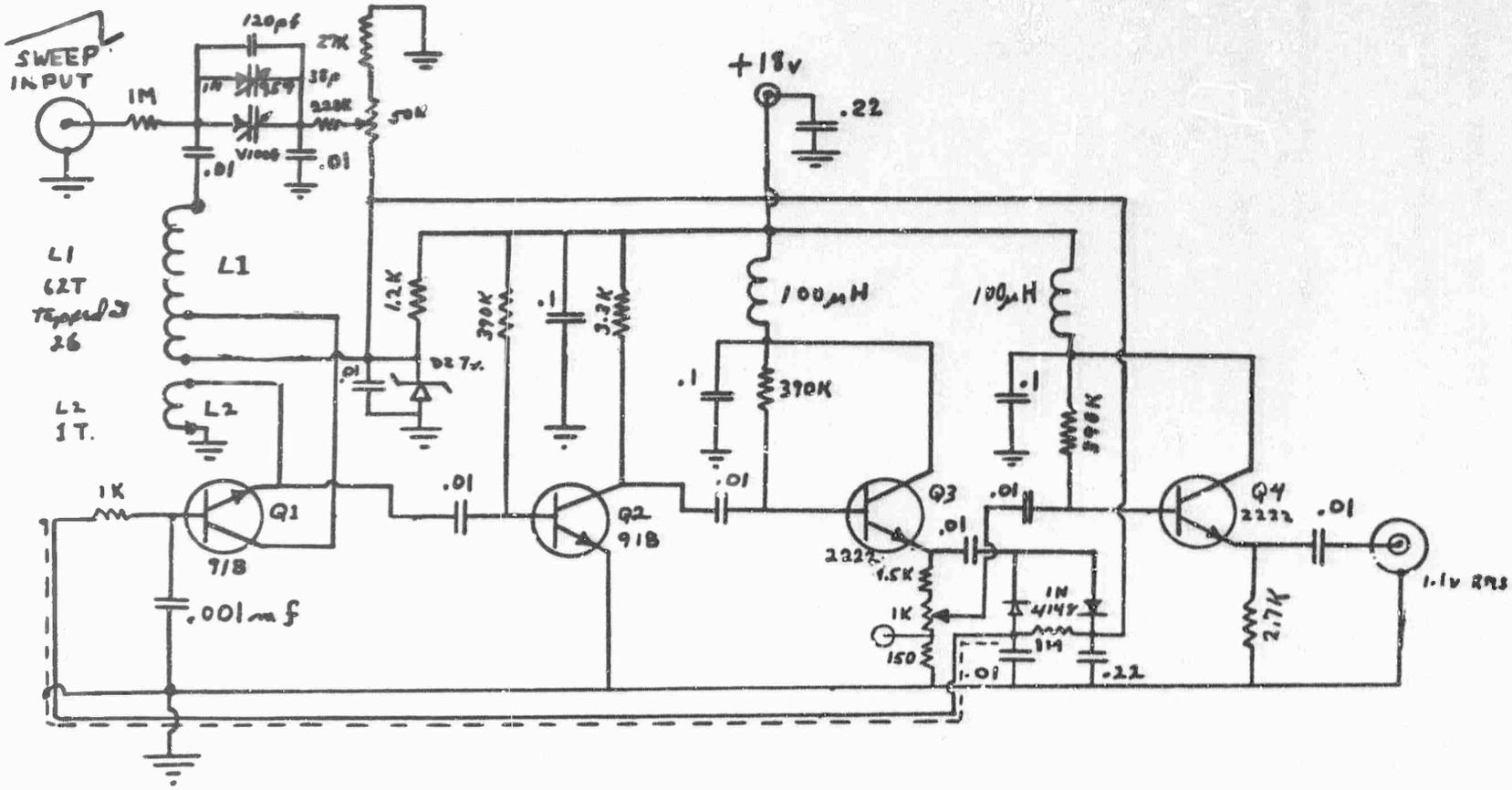

Figure 3-12.- Voltage Controlled, Swept Generator

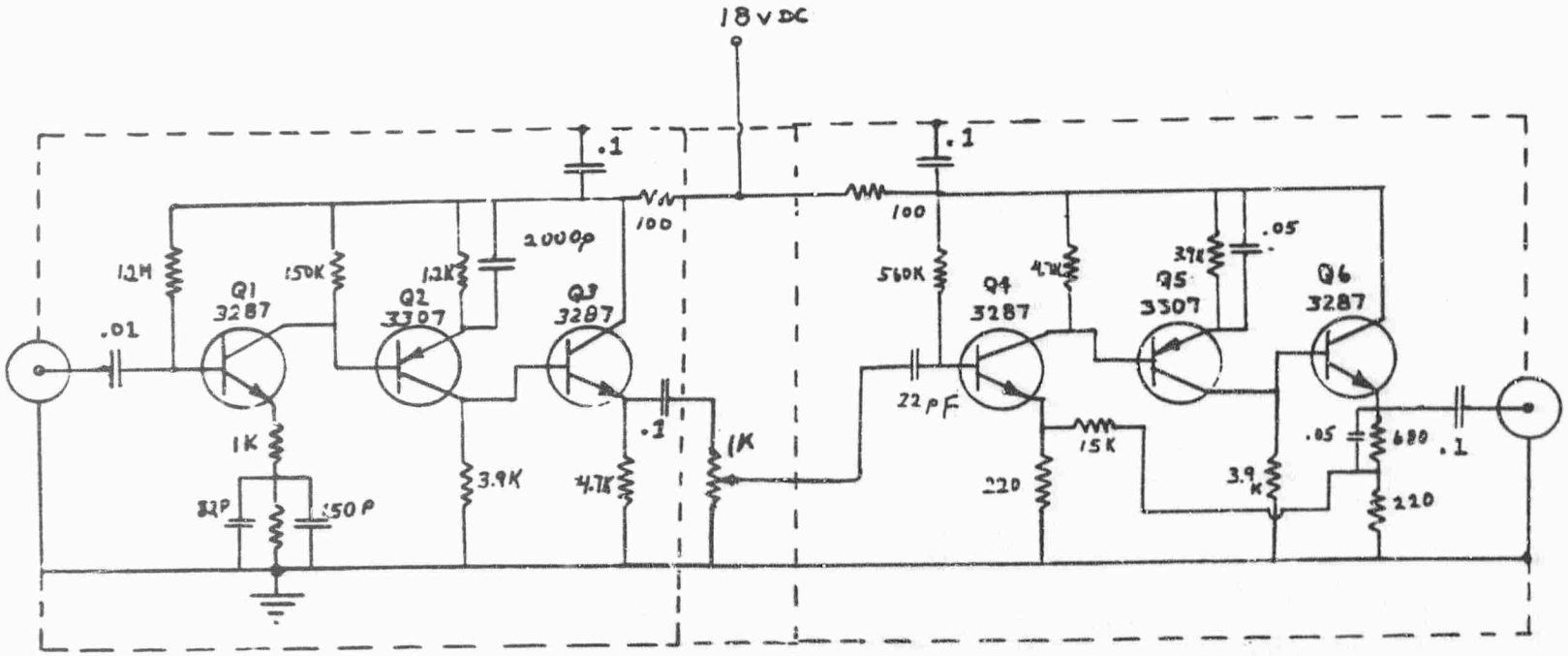

Figure 3-13 - Null Amplifier

The frequency of the voltage controlled crystal oscillator VCXO could be varied over a range of ±20 Hz around 1 MHz by a control voltage that varied from 2 to 6 volts.

The unit had a maximum undistorted output of 2.2 volts into a high impedance (about 1K).

The circuit diagram is shown in Figure 3-14.

The final amplifiers have a very flat frequency response to minimize spurious phase pulling and the circuit includes an automatic gain control (AGC) loop to keep the output level stable. The control voltage was applied to a varicap, slightly altering the capacitive loading of the crystal thereby "pulling" its frequency.

When this unit was constructed, it was intended that it be included in the modifications to Promant; however, it was abandoned when the theoretical and experimental proofs of the futility of pulsing were obtained.

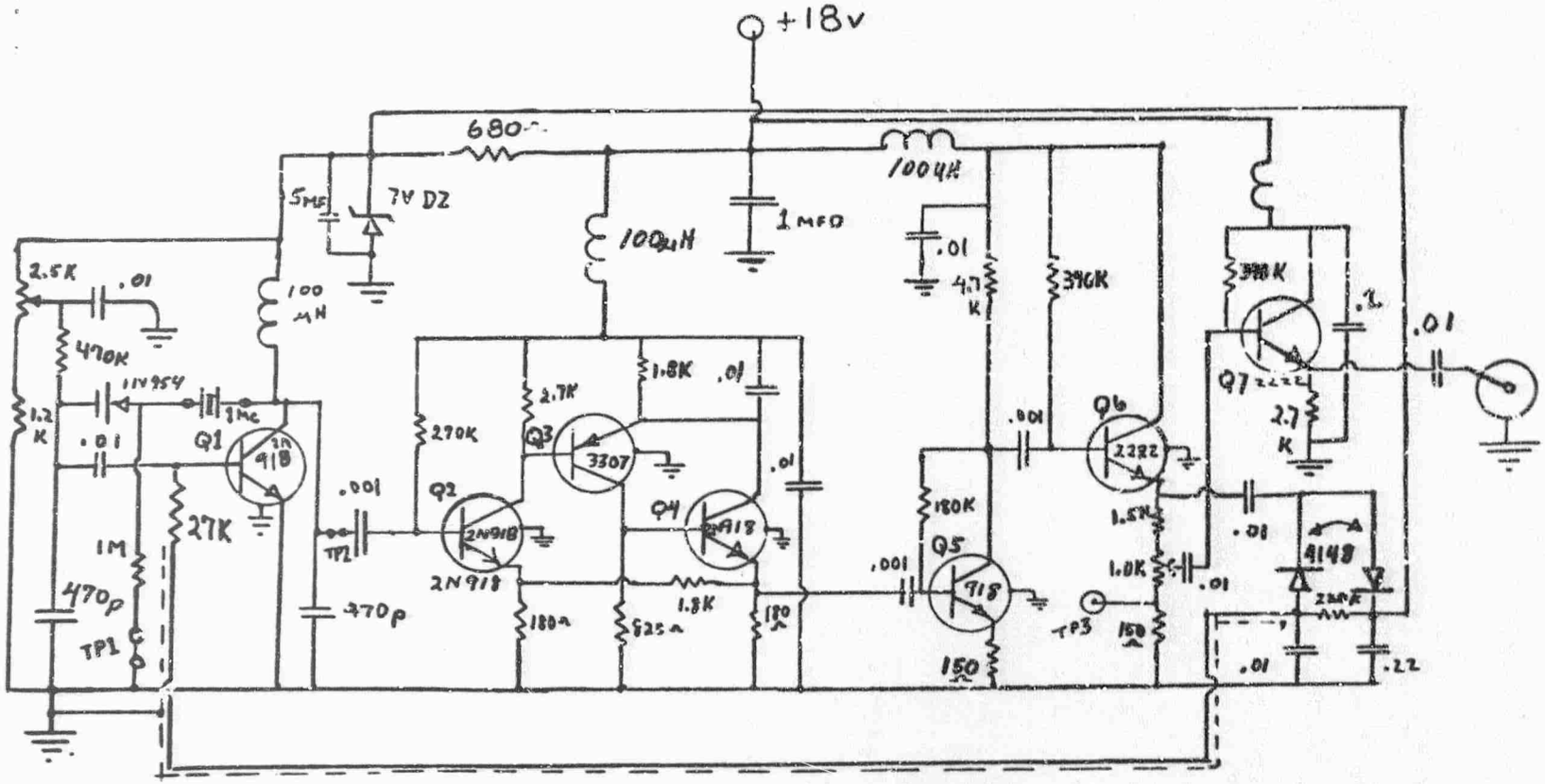

Figure 3-14 - Voltage Controlled Crystal Oscillator

SECTION 4

C O N C L U S I O N S

The most important conclusion reached during this study and investigation was that pulsed operation of the NMR oscillator offered no advantages over CW operation. This problem was investigated in considerable detail, both theoretically and experimentally. The results of these investigations (presented in Section 2.1.3) were unambiguous and permitted only the conclusion stated above.

Excellent success was attained in developing techniques for providing VLF tuning. The magnetic heterodyning technique using eddy current flux-cancelling coils for μ-switching extended the frequency range of the antenna to more than 10^4 Hz. No significant improvement in sensitivity was observed without using magnetic heterodyning.

A P P E N D I X A

TYPICAL SENSITIVITY DATA

Figure A-1 is a reproduction of an actual recording of the data used to obtain the 300 Hz data point on Figure 3-8. The signal occurring between the letters D and E represents a magnetic field of 2.14×10^{-5} gauss at 300 Hz. For this measurement, no magnetic heterodyning was used. The maser power was 2×10^{-10} watts.

A typical magnetic heterodyning measurement is shown in Figure A-2. The signal shown is caused by a magnetic field of 16×10^{-5} gauss at a frequency of 10^4 Hz. The excess noise occurring while the oscillating magnetic field is present results from the relative instability of the two oscillators used to generate the field and used for a local oscillator, respectively. The maser power during this measurement was 8×10^{-11} watts. This data was used to obtain the data point (with heterodyning) at 10 kHz in Figure 3-8.

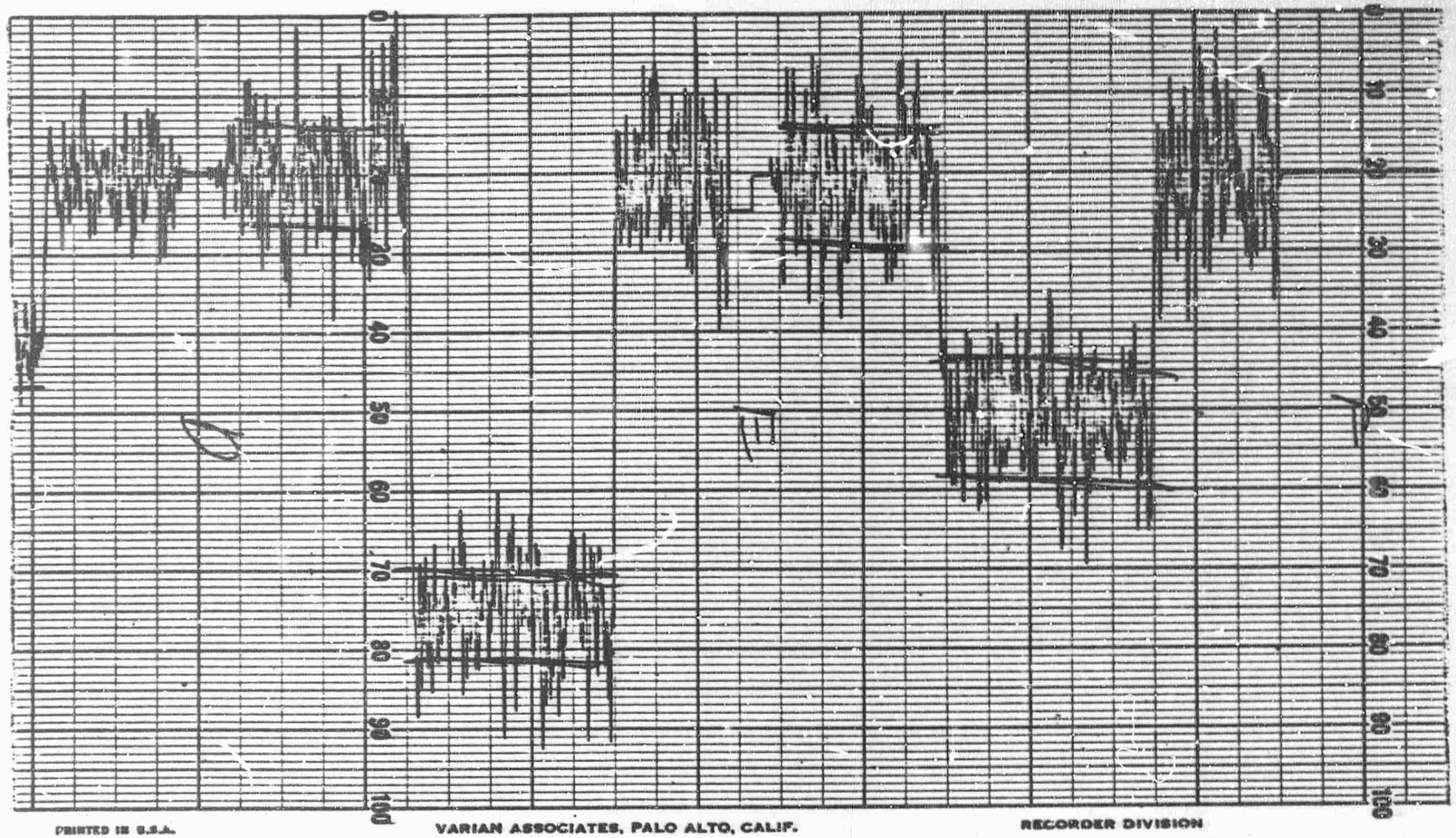

Figure A-1 - Typical Sensitivity Data

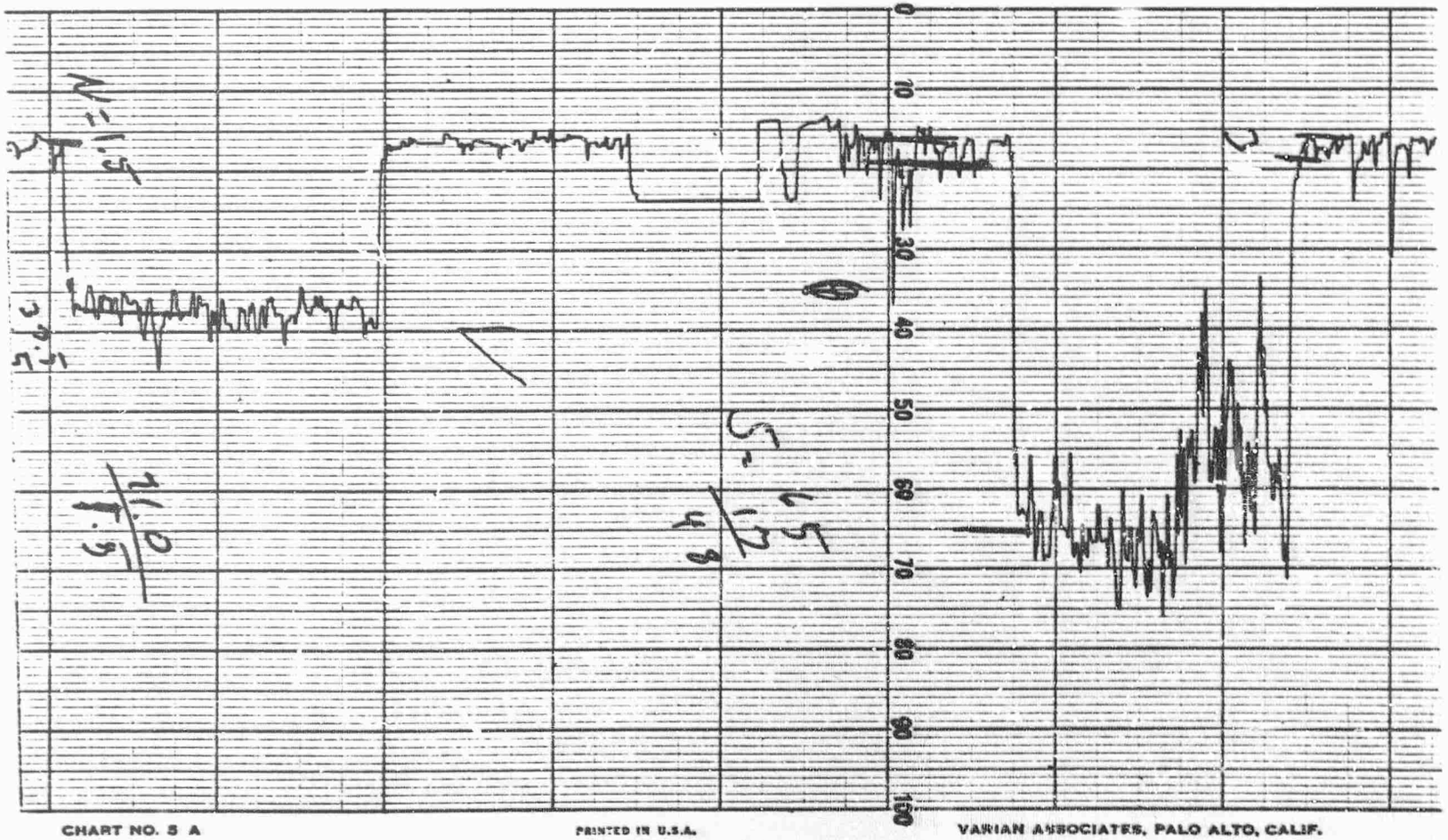

Figure A-2 - Typical Data with Heterodyning

UNCLASSIFIED
Security Classification

DOCUMENT CONTROL DATA - R&D
(Security classification of title, body of abstract and indexing annotation must be entered when the overall report is classified)

1. ORIGINATING ACTIVITY (Corporate author) National Company, Inc. Melrose, Mass. 02176	2a. REPORT SECURITY CLASSIFICATION Unclassified 2b. GROUP

3. REPORT TITLE
Study and Investigation of an Improved Proton Maser Antenna

4. DESCRIPTIVE NOTES (Type of report and inclusive dates)
Final Report

5. AUTHOR(S) (Last name, first name, initial)
Thornburg, Clarence O.
Webster, Jonathan
Guttrich, Gordon

6. REPORT DATE October 1966	7a. TOTAL NO. OF PAGES 66	7b. NO. OF REFS 10
8a. CONTRACT OR GRANT NO. AF30(602)-3742 b. PROJECT NO. 4519 c. Task No. 451903 d.	9a. ORIGINATOR'S REPORT NUMBER(S) 9b. OTHER REPORT NO(S) (Any other numbers that may be assigned this report) RADC-TR-66-545	

10. AVAILABILITY/LIMITATION NOTICES
This document is subject to special export controls and each transmittal to foreign governments or foreign nationals may be made only with prior approval of RADC (EMLI), GAFB, N. Y. 13440.

11. SUPPLEMENTARY NOTES Walter J. Bushunow Project Engineer	12. SPONSORING MILITARY ACTIVITY Rome Air Development Center (EMCRA) Griffiss Air Force Base, New York 13440

13. ABSTRACT

The report presents results of a study and investigation of techniques for improving the performance of a Proton Maser Antenna, a new sensor technique for the ELF-VLF frequency region, developed under Contract AF30(602)-2908. Problems of increasing threshold sensitivity and providing band tuning of the antenna were considered under the present effort.

The heterodyne method was utilized for VLF tuning. This method uses eddy current flux-cancelling coils for μ-switching purposes. The incoming signal is magnetically chopped at a predetermined rate and is translated into a fixed intermediate frequency. By the utilization of this technique, the frequency range of the antenna is extended from 100 Hz to 10^4 Hz without appreciable degradation in sensitivity.

Partial success was achieved in the effort concerned with increasing the sensitivity of the antenna. A new coil box was constructed in order to increase the sample flow volume by 50%. This undertaking should theoretically increase the sensitivity by 22%. The Overhauser enhancement was increased from A=-50 to A=-90. This improved enhancement corresponds to a 25% theoretical increase in sensitivity. Studies conducted on increasing antenna sensitivity by pulsed mode operation were unsuccessful. These studies indicated that an increase factor of two instead of the expected 38 db could be realized. An attempt was undertaken
(over)

DD FORM 1 JAN 64 1473

UNCLASSIFIED
Security Classification